AD 268 909

DISCLAIMER NOTICE

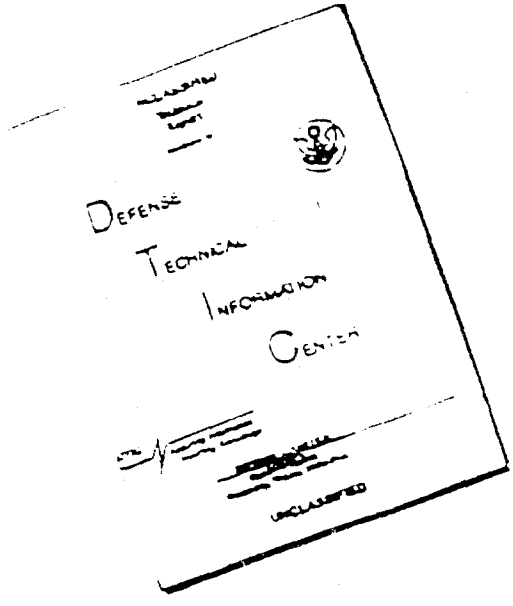

THIS DOCUMENT IS BEST QUALITY AVAILABLE. THE COPY FURNISHED TO DTIC CONTAINED A SIGNIFICANT NUMBER OF PAGES WHICH DO NOT REPRODUCE LEGIBLY.

DEPARTMENT OF THE NAVY
DAVID TAYLOR MODEL BASIN

HYDROMECHANICS

AERODYNAMICS

STRUCTURAL MECHANICS

APPLIED MATHEMATICS

INVESTIGATION ON THE INFLUENCE OF STIFFENER SIZE ON THE BUCKLING PRESSURES OF CIRCULAR CYLINDRICAL SHELLS UNDER HYDROSTATIC PRESSURE

by

James A. Nott

STRUCTURAL MECHANICS LABORATORY

RESEARCH AND DEVELOPMENT REPORT

December 1961

Report 1600

INVESTIGATION ON THE INFLUENCE OF STIFFENER SIZE ON THE BUCKLING PRESSURES OF CIRCULAR CYLINDRICAL SHELLS UNDER HYDROSTATIC PRESSURE

by

James A. Nott

This report is based on a thesis investigation submitted to the Faculty of The College of Engineering of the George Washington University in partial satisfaction of the requirements for the degree of Master of Science in Engineering.

December 1961

Report 1600
S-F013 03 02

TABLE OF CONTENTS

LIST OF TABLES

LIST OF ILLUSTRATIONS

ABSTRACT

A theoretical derivation is given for elastic and plastic buckling of stiffened circular cylindrical shells under external hydrostatic pressure. The theory accounts for variable shell stresses, as influenced by the circular stiffeners, and critical buckling pressures are obtained for simple support conditions at the shell-frame junctures. Methods are given for the determination of collapse pressures for both elastic and plastic asymmetric buckling by iteration and numerical minimization. The theory is applicable to shells made either of strain-hardening or elastic-perfectly plastic materials.

Using the theory developed in this report it is shown that a variation in stiffener size can change the buckling pressures. Test data from high-strength steel and aluminum cylinders are presented which show theoretical and experimental collapse pressures to agree within approximately 6 per cent.

INVESTIGATION ON THE INFLUENCE OF STIFFENER SIZE ON THE BUCKLING PRESSURES OF CIRCULAR CYLINDRICAL SHELLS UNDER HYDROSTATIC PRESSURE

INTRODUCTION

Since the USS HOLLAND was launched in 1911, the Navy has been interested in the design of reinforced cylinders for submarine structures. Various theoretical formulae have been established for the purpose of design to calculate a collapse pressure for a specific geometry, and experimental models have been constructed and tested under external hydrostatic pressure to check the theories.

Collapse pressures for various modes of failure must be determined before the naval architect can arrive at a rational design. The collapse of a cylindrical shell stiffened by circular frames may occur in one of three modes depending upon its geometry. Considering a given shell-thickness to shell-diameter ratio, failure may occur by

1. General instability,
2. Asymmetric shell buckling, or
3. Axisymmetric shell collapse.

General instability occurs when the size of the frames

is critical for a given frame spacing, resulting in collapse of the frames together with the shell. Failure may occur along several frames or it may occur over the entire length of a compartment. Shell buckling occurs when frame size is sufficient to prevent general instability, but the frame spacing is critical. In this type of shell failure a series of asymmetrical lobes form in the shell between frames. Axisymmetric shell collapse occurs when the frame size is sufficient to prevent general instability and the diameter-frame spacing ratio is sufficient to prevent shell buckling. Failure occurs by yielding of the shell material, resulting in an axisymmetric fold in the shell between frames.

Theoretical solutions for the elastic instability of cylindrical shells have been derived by Mises (1) and Sanden and Tölke (2), and their solutions apply when stresses in the shell are linear when buckling occurs. The problem of plastic collapse has been recently treated by Reynolds (3) for the asymmetric mode of failure and by Lunchick (4 and 5) for the axisymmetric mode. In their solutions the nonlinear effect of the stress-strain curve in the elastic-plastic region is considered.

A subject of current interest to the naval architect is that of the effect of the size of the reinforcing circular frames on the asymmetric shell buckling of cylindrical shells under external hydrostatic pressure. This problem becomes important in the design of submarines, since it is advantageous

to have the structural material in the shell and frame so distributed that it gives a maximum collapse pressure for a minimum weight.

In this report a theoretical analysis of the asymmetric shell-buckling mode of a circular framed cylindrical shell loaded under external uniform lateral and axial pressure is presented. Gerard's (6) equations of equilibrium for plastic buckling are solved using realistic expressions for stresses in the shell determined by the Salerno-Pulos (7) theory, which accounts for the effect of circular frames. Since the stresses at the shell-frame junctures are in the elastic-plastic range prior to plastic collapse, simple support is assumed at the shell-frame junctures. A series of curves showing the theoretical effect of frame size for specific geometries of interest to the naval architect is also presented.

The analysis presented in this paper is an extension of Reynolds' (3) solution. It differs from Reynolds' (3) work in that the plasticity coefficients in Gerard's (6) equations of equilibrium are expressed in terms of variable shell stresses determined by Salerno and Pulos (7). The feature of variable shell stresses becomes important in this problem, as a change in frame size will produce a change in shell stresses.

Many present structures are being constructed from materials such as high-strength steel and aluminum, which

exhibit a nonlinear type stress-strain curve in the elastic-plastic region. Therefore, this analysis is outlined for strain-hardening materials. Experimental results are shown for comparison with the theory.

CHAPTER I

THEORY OF BUCKLING

Various investigators have considered the critical buckling pressure of a circular framed reinforced cylinder loaded under external uniform pressure. Mises (1) considered the case of a cylindrical shell between two bulkheads without intermediate stiffening rings, for which he derived an elastic analysis assuming the prebuckling stresses (stresses preceding bifurcation of equilibrium) to be $\sigma_x = \frac{pR}{2h}$ and $\sigma_s = \frac{pR}{h}$. Later Sanden and Tölke (2) considered the effect of the stiffening rings and derived an elastic analysis for hydrostatic loading. Reynolds' (3) analysis considered both elastic and plastic buckling for the case with stiffening rings. In Reynolds' (3) solution the stresses $\frac{pR}{2h}$ and $\frac{pR}{h}$ were used to calculate Gerard's (6) plasticity coefficients. Reynolds (3) then used stresses, as shown by Sanden and Günther (8), to define prebuckling stresses in the equations of equilibrium.

Plastic-Buckling Theory

In the case of circular cylindrical shells loaded under external lateral and axial uniform pressure (external hydrostatic pressure) the two principal axes are parallel and perpendicular to the longitudinal axis of the cylinder (see Figure 1).

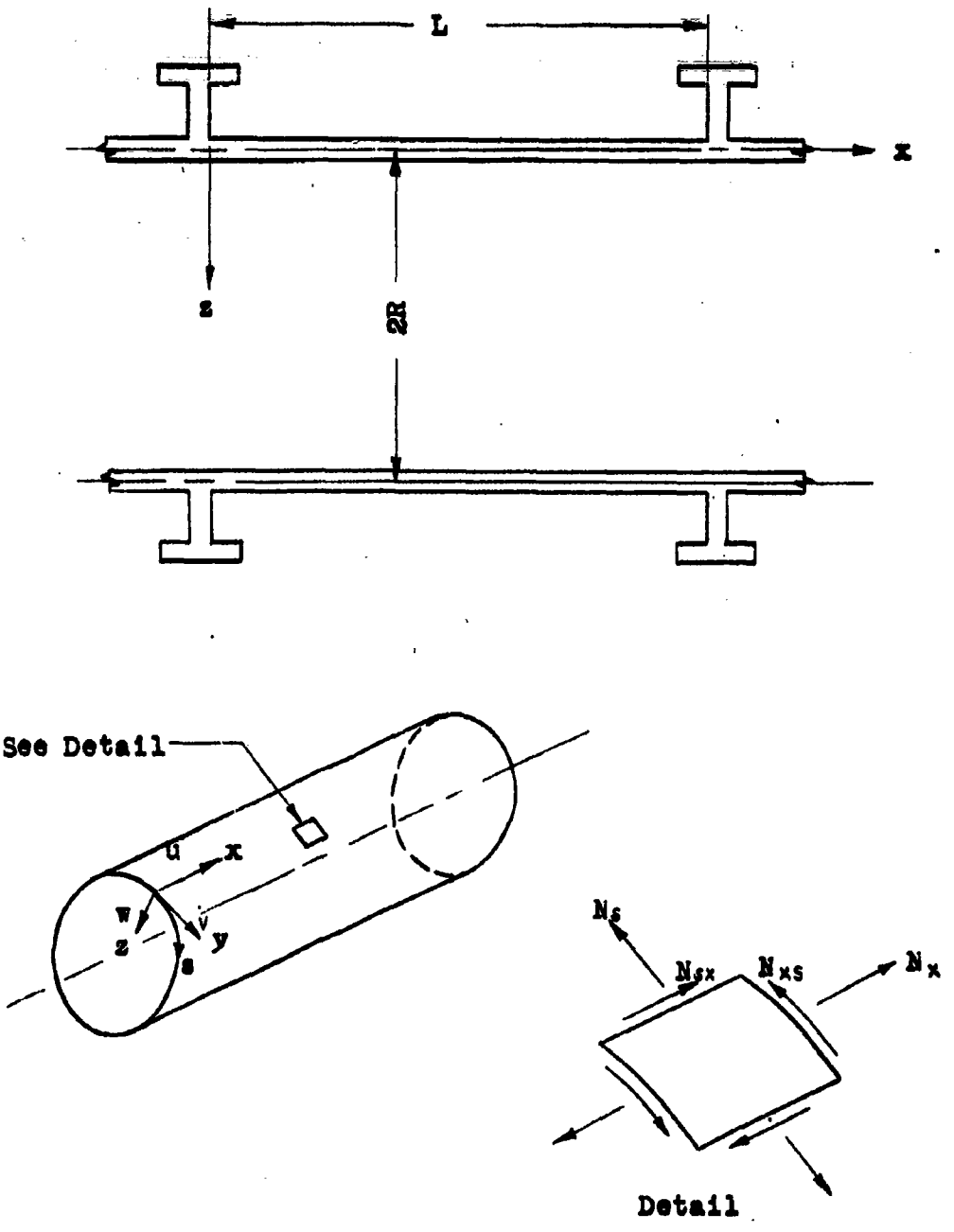

Figure 1 - Coordinate System for Stiffened Cylindrical Shell

Therefore, the shear stress is given by

$$\tau = \frac{N_{x\varsigma}}{h} = 0. \qquad [1]$$

Using membrane stress theory, which considers only stresses on the middle surface of the shell (neglecting bending), the longitudinal membrane stress can be determined from the equation of equilibrium in the longitudinal direction:

$$\sigma_x = \frac{N_x}{h} = \frac{pR}{2h}, \qquad [2]$$

where N_x is the longitudinal force per unit length in the longitudinal direction.

The circumferential membrane stress can be obtained by the analysis of Salerno and Pulos (7) who express the stress as follows:

$$\sigma_s = \phi \frac{pR}{h}, \qquad [3]$$

where

$$\phi = \phi(p).$$

In the theory of buckling, a certain stress condition at a point in the shell is assumed to reach a limiting value at the onset of collapse. The circumferential stress varies with x and the stress condition is assumed to be most critical at midbay; therefore, the stress is taken at the midbay, midplane fiber location. The function, ϕ, which determines the axisymmetric stress at this location of a circular framed cylindrical shell loaded under external hydrostatic

pressure is given by the theory of Salerno and Pulos (7) and expressed by Krenzke and Short (9) as follows:

$$\phi = 1 - \frac{(1 - \frac{\nu}{2})\alpha_1 F_2}{\alpha_1 + \beta + F_1(1 - \beta)}, \qquad [4]$$

where α_1 is the ratio of frame area to shell area and is expressed as

$$\alpha_1 = \frac{A_F}{h L_F}, \qquad [4a]$$

and β is the ratio of faying width of the stiffener to bay length and is expressed as

$$\beta = \frac{b}{L_F}, \qquad [4b]$$

and

A_F is the effective area of the frame obtained by multiplying the true area of the frame by R/R_F for internally framed cylinders and $(R/R_F)^2$ for externally framed cylinders,

h is the shell thickness,

L_F is the center to center frame spacing,

b is the effective faying width of the stiffener in contact with the shell,

L is the clear span frame spacing, L_F - b,

R is the radius to the midplane surface of the shell,

R_F is the radius to the c.g. of the frame,

ν is Poisson's ratio,

E is Young's modulus, and

p is external uniform pressure.

The functions F_1 and F_2 are defined as follows:

$$F_1 = \left(\frac{4}{\theta}\right)\left[\frac{\cosh^2\eta_1\theta - \cos^2\eta_2\theta}{\frac{\cosh\eta_1\theta\,\sinh\eta_1\theta}{\eta_1} + \frac{\cos\eta_2\theta\,\sin\eta_2\theta}{\eta_2}}\right]$$

$$F_2 = \frac{\frac{\cosh\eta_1\theta\,\sin\eta_2\theta}{\eta_2} + \frac{\sinh\eta_1\theta\,\cos\eta_2\theta}{\eta_1}}{\frac{\cosh\eta_1\theta\,\sinh\eta_1\theta}{\eta_1} + \frac{\cos\eta_2\theta\,\sin\eta_2\theta}{\eta_2}}, \qquad [4c]$$

in which θ is the shell flexibility parameter and is expressed as

$$\theta = \sqrt[4]{3(1-\nu^2)}\,\frac{L}{\sqrt{Rh}}, \qquad [4d]$$

and

$$\eta_1 = \frac{1}{2}\sqrt{1-\gamma_1}$$
$$\eta_2 = \frac{1}{2}\sqrt{1+\gamma_1}, \qquad [4e]$$

where γ_1 is a measure of the beam-column effect and is expressed as

$$\gamma_1 = \frac{p}{2E}\left(\frac{R}{h}\right)^2\sqrt{3(1-\nu^2)}. \qquad [4f]$$

When $\gamma_1 = 0$ (no beam-column effect), the above expressions for the Salerno-Pulos (7) stress at the midbay, midplane location reduce to the Sanden-Günther (8) theory.

For simplification, curves are shown in Appendix A for the evaluation of the functions, F_1 and F_2. It has been shown by Krenzke and Short (9) that stresses computed using these curves are within 0.2 per cent of those computed by precise calculations.

In this analysis, the plasticity coefficients are expressed in terms of σ_x and σ_s and the assumption of Reynolds (3) that $\sigma_s = 2\sigma_x$ is not made. Utilizing Gerard's (6) plasticity coefficients and general differential equations of equilibrium for the plastic region (see Appendix B) and using Equation 1, one will find that the coefficients involving the shear stress vanish; i.e.

$$C_{13} = C_{31} = C_{23} = C_{32} = 0. \qquad [5]$$

Therefore, the equilibrium equations can be written as

$$\left(1-\alpha\frac{\sigma_x^2}{4}\right)\frac{\partial^2 u}{\partial x^2} + \frac{1}{4}\frac{\partial^2 u}{\partial s^2} + \left(\frac{3}{4}-\alpha\frac{\sigma_x\sigma_s}{4}\right)\frac{\partial^2 v}{\partial x\partial s} + \left(\frac{1}{2}-\alpha\frac{\sigma_x\sigma_s}{4}\right)\frac{1}{R}\frac{\partial w}{\partial x} = 0$$

$$\left(1-\alpha\frac{\sigma_s^2}{4}\right)\frac{\partial^2 v}{\partial s^2} + \frac{1}{4}\frac{\partial^2 v}{\partial x^2} + \left(\frac{3}{4}-\alpha\frac{\sigma_x\sigma_s}{4}\right)\frac{\partial^2 u}{\partial x\partial s} + \left(1-\alpha\frac{\sigma_s^2}{4}\right)\frac{1}{R}\frac{\partial w}{\partial s} = 0 \qquad [6]$$

$$D\left[\left(1-\alpha\frac{\delta_x^2}{4}\right)\frac{\partial^4 w}{\partial x^4} + \left(2-\alpha\frac{\delta_x\delta_s}{2}\right)\frac{\partial^4 w}{\partial x^2\partial s^2}\right.$$
$$\left.+\left(1-\alpha\frac{\delta_s^2}{4}\right)\frac{\partial^4 w}{\partial s^4}\right] + \frac{4E\delta_s}{3R}\left[\left(\frac{1}{2}-\alpha\frac{\delta_x\delta_s}{4}\right)\frac{\partial^2 v}{\partial x\partial s}\right.$$
$$\left.+\left(1-\alpha\frac{\delta_s^2}{4}\right)\left(\frac{\partial v}{\partial s}+\frac{w}{R}\right)\right] + N_x\frac{\partial^2 w}{\partial x^2} \qquad \text{[6] cont'd}$$
$$+ N_s\frac{\partial^2 w}{\partial s^2} + p = 0.$$

It is obvious that an exact solution to Equations 6 is not readily obtained and an approximate solution must be sought.

If simple support conditions are assumed at the shell-frame junctures, the boundary conditions which must be satisfied are

$$w\Big|_{x=0} = w\Big|_{x=L} = 0 \qquad [7]$$

and

$$\frac{\partial^2 w}{\partial x^2}\Big|_{x=0} = \frac{\partial^2 w}{\partial x^2}\Big|_{x=L} = 0. \qquad [8]$$

Simple support implies that the frames offer no restraint to longitudinal bending in the shell at the shell-frame junctures. This assumption at the boundary may be justified by concluding that, when plastic behavior begins in the shell at the shell-frame junctures, the frames produce little restraint against rotation of the shell. The general solution of Equations 6 satisfying the boundary conditions, Equations 7 and 8, can be expressed as

$$u = A_0 \sin ks \cos \lambda x$$
$$v = B_0 \cos ks \sin \lambda x \qquad [9]$$
$$w = C_0 \sin ks \sin \lambda x ,$$

where the mode shape coefficients, k and λ, are expressed as

$$k = n/R \text{ and } \lambda = m\pi/L,$$

in which m and n are numbers of half-waves of the buckling configuration in the longitudinal and circumferential directions, respectively. The quantities u, v, and w in Equations 9 represent small displacements in the x, y, and z directions, respectively (see Figure 1). Substituting these displacements into Equations 6, we obtain three linear equations:

$$-\left[\lambda^2\left(1-\alpha\frac{\sigma_x^2}{4}\right)+\frac{k^2}{4}\right]A_0 - k\lambda\left(\frac{3}{4}-\alpha\frac{\sigma_x\sigma_\varepsilon}{4}\right)B_0 + \frac{\lambda}{R}\left(\frac{1}{2}-\alpha\frac{\sigma_x\sigma_\varepsilon}{4}\right)C_0 = 0$$

$$-k\lambda\left(\frac{3}{4}-\alpha\frac{\sigma_x\sigma_\varepsilon}{4}\right)A_0 - \left[k^2\left(1-\alpha\frac{\sigma_\varepsilon^2}{4}\right)+\frac{\lambda^2}{4}\right]B_0 + \frac{k}{R}\left(1-\alpha\frac{\sigma_\varepsilon^2}{4}\right)C_0 = 0$$

$$-\frac{4E_s h}{3R}\left[\lambda\left(\frac{1}{2}-\alpha\frac{\sigma_x\sigma_\varepsilon}{4}\right)A_0 + k\left(1-\alpha\frac{\sigma_\varepsilon^2}{4}\right)B_0\right] \qquad [10]$$
$$+\left\{D\left[\lambda^4\left(1-\alpha\frac{\sigma_x^2}{4}\right)+\lambda^2k^2\left(2-\alpha\frac{\sigma_x\sigma_\varepsilon}{2}\right)+k^4\left(1-\alpha\frac{\sigma_\varepsilon^2}{4}\right)\right] + \frac{4E_s h}{3R^2}\left(1-\alpha\frac{\sigma_\varepsilon^2}{4}\right) - \lambda^2N_x - k^2N_s\right\}C_0 = \frac{-p}{\sin ks \sin \lambda x} .$$

Equations 10 express the displacements u, v, and w, and their derivatives, in terms of the arbitrary mode shape parameters, A_o, B_o, and C_o. The stability criterion assumes the shell will buckle when the displacements increase beyond limit. To satisfy this criterion, the determinant of the coefficients of A_o, B_o, and C_o must be set equal to zero. Equating this determinant to zero, we obtain the characteristic equation:

$$
\begin{aligned}
&-\left[\lambda^2\left(1-\alpha\frac{\sigma_x^2}{4}\right)+\frac{k^2}{4}\right]\left\{-\left[k^2\left(1-\alpha\frac{\sigma_s^2}{4}\right)+\frac{\lambda^2}{4}\right]\right. \\
&\left\{D\left[\lambda^4\left(1-\alpha\frac{\sigma_x^2}{4}\right)+\lambda^2k^2\left(2-\alpha\frac{\sigma_x\sigma_s}{2}\right)+k^4\left(1-\alpha\frac{\sigma_s^2}{4}\right)\right]\right. \\
&\left.+\frac{\psi}{R}\left(1-\alpha\frac{\sigma_s^2}{4}\right)-\lambda^2N_x-k^2N_s\right\}+\frac{\psi k^2}{R}\left(1-\alpha\frac{\sigma_s^2}{4}\right)^2\Bigg] \\
&+\frac{k\lambda}{2}\left(\frac{3}{2}-\alpha\frac{\sigma_x\sigma_s}{2}\right)\left\{-\frac{k\lambda}{2}\left(\frac{3}{2}-\alpha\frac{\sigma_x\sigma_s}{2}\right)\left\{D\left[\lambda^4\left(1-\alpha\frac{\sigma_x^2}{4}\right)\right.\right.\right. \\
&\left.\left.+\lambda^2k^2\left(2-\alpha\frac{\sigma_x\sigma_s}{2}\right)+k^4\left(1-\alpha\frac{\sigma_s^2}{4}\right)\right] \qquad [11] \\
&+\frac{\psi}{R}\left(1-\alpha\frac{\sigma_s^2}{4}\right)-\lambda^2N_x-k^2N_s\Bigg\}+\frac{\psi k\lambda}{2R}\left(1-\alpha\frac{\sigma_s\sigma_x}{2}\right)\left(1-\alpha\frac{\sigma_s^2}{4}\right)\Bigg\} \\
&+\frac{\lambda}{2R}\left(1-\alpha\frac{\sigma_x\sigma_s}{2}\right)\left\{\frac{\psi k^2\lambda}{2}\left(\frac{3}{2}-\alpha\frac{\sigma_x\sigma_s}{2}\right)\left(1-\alpha\frac{\sigma_s^2}{4}\right)\right. \\
&\left.-\frac{\psi\lambda}{2}\left(1-\alpha\frac{\sigma_x\sigma_s}{2}\right)\left[k^2\left(1-\alpha\frac{\sigma_s^2}{4}\right)+\frac{\lambda^2}{4}\right]\right\}=0,
\end{aligned}
$$

where

$$\psi=\frac{4E_sh}{3R}.$$

Equation 11 implicitly expresses the pressure as a function of σ_x, σ_s, N_x, and N_s. Noting that

$$N_x = \sigma_x h = \frac{pR}{2} \qquad [12]$$

and

$$N_s = \sigma_s h = \phi p R, \qquad [13]$$

we can put Equation 11 in the form $p = f(\sigma_x, \sigma_s)$.

Nadai (10) and Hoffman and Sachs (11) show that an effective stress, σ_i, and an effective strain, ϵ_i, can be determined by the octahedral shear-stress theory:

$$\sigma_i^2 = \sigma_x^2 + \sigma_s^2 - \sigma_x \sigma_s + 3\tau^2 \qquad [14]$$

and

$$\epsilon_i^2 = \frac{4}{3}\left(\epsilon_x^2 + \epsilon_s^2 + \epsilon_x \epsilon_s + \frac{\gamma^2}{4}\right). \qquad [15]$$

If we utilize the ratio of the circumferential and longitudinal stresses, we obtain

$$\frac{\sigma_s}{\sigma_x} = \frac{\phi \frac{pR}{h}}{\frac{pR}{2h}} = 2\phi. \qquad [16]$$

For principal stresses and strains $\tau = \gamma = 0$, and Equation 14 with the use of Equation 16 can be written in the following three forms:

$$\sigma_x^2 = \frac{\sigma_i^2}{4\phi^2 - 2\phi + 1}$$

$$\sigma_s^2 = \frac{4\phi^2 \sigma_i^2}{4\phi^2 - 2\phi + 1} \qquad [17]$$

$$\sigma_x \sigma_s = \frac{2\phi \sigma_i^2}{4\phi^2 - 2\phi + 1} .$$

From Appendix B the effective stress parameter is expressed as

$$\alpha = \frac{3}{\sigma_i^2}\left(1 - \frac{E_t}{E_s}\right) , \qquad [18]$$

where the tangent and secant moduli are

$$E_t = \frac{d\sigma_i}{d\epsilon_i} \qquad [19]$$

and

$$E_s = \frac{\sigma_i}{\epsilon_i} , \qquad [20]$$

respectively.

The values σ_i and ϵ_i in Equations 14, 15, 19, and 20 are assumed to be the same as those in a uniaxial compression test, and therefore, E_t and E_s can be obtained directly from a stress-strain curve of the material.

Equations 17 and 18 can be written as

$$\alpha \frac{\sigma_x^2}{4} = CM,$$

$$\alpha \frac{\sigma_s^2}{4} = 4\phi^2 CM, \qquad [21]$$

and

$$\alpha \frac{\sigma_x \sigma_s}{2} = 4\phi CM,$$

where the coefficient, C, is

$$C = \frac{3}{4(4\phi^2 - 2\phi + 1)}, \qquad [21a]$$

and the moduli parameter, M, is

$$M = \left(1 - \frac{E_t}{E_s}\right). \qquad [21b]$$

Substituting Equations 21 into the characteristic-value equation, Equation 11, the plastic-buckling pressure, p_p, can be expressed after simplification as

$$p_p = \frac{4D[A_1 - (CM)X_1 + (CM)^2 X_2] + \frac{E_s h \lambda^4}{R^2}}{R\left(\frac{\lambda^2}{2} + k^2\phi\right)\left\{(k^2+\lambda^2)^2 - 3M\left[\frac{\left(\frac{\lambda^2}{2} - k^2\phi\right)^2}{4\phi^2 - 2\phi + 1} + \lambda^2 k^2\right]\right\}}, \qquad [22]$$

where

$$X_1 = A_2 - A_3\phi + A_4\phi^2$$

$$X_2 = A_5 + A_6\phi + A_7\phi^2 - A_8\phi^3 + A_9\phi^4,$$

and

$$
\begin{aligned}
A_1 &= \tfrac{1}{4}(k^2+\lambda^2)^4 \\
A_2 &= \tfrac{1}{2}\lambda^2(k^2+\lambda^2)^2(2k^2+\lambda^2) \\
A_3 &= 2k^2\lambda^2(k^2+\lambda^2)^2 \\
A_4 &= 2k^2(k^2+\lambda^2)^2(k^2+2\lambda^2) \\
A_5 &= \tfrac{1}{4}\lambda^6(4k^2+\lambda^2) \\
A_6 &= 2k^2\lambda^4(2k^2-\lambda^2) \\
A_7 &= 2k^2\lambda^2(2k^2-\lambda^2)(k^2-2\lambda^2) \\
A_8 &= 8k^4\lambda^2(k^2-2\lambda^2) \\
A_9 &= 4k^6(k^2+4\lambda^2).
\end{aligned}
\qquad [23]
$$

Since ϕ is a function of the pressure (see Equation 3), Equation 22 represents a transcendental equation for the pressure, p_p. The plastic-buckling pressure, p_p, in Equation 22 defines a range of collapse pressures for different values of σ_1 beyond the elastic limit. The flexural rigidity of the shell, D, in Equation 22 is given by

$$D = \frac{E_s h^3}{12(1-\nu^2)}, \qquad [24]$$

where Poisson's ratio, ν, in the elastic-plastic region is shown by Gerard and Wildhorn (12) to be

$$\nu = \frac{1}{2} - \frac{E_s}{E}\left(\frac{1}{2} - \nu_e\right). \qquad [25]$$

Although the equilibrium equations were derived for a constant Poisson's ratio of 1/2, Equation 25 is used in Equation 24 to account for the fact that Poisson's ratio increases from its value ν_e in the elastic region to an upper limit of 1/2 for an isotropic, incompressible material. Poisson's ratio in the elastic region is usually assumed to be 0.3 for most structural materials. For a check, a rigorous comparison shows that Equation 22 with $\phi = 1$ reduces identically to Reynolds' [(3), p.4] solution for $\sigma_x/\sigma_s = 1/2$.

Equation 14 can also be used to determine the relationship between the prebuckling stress condition in the shell and the applied pressure. Solving Equation 14 for p, one obtains:

$$p_s = \frac{2h\sigma_1}{R\sqrt{4\phi^2 - 2\phi + 1}} . \qquad [26]$$

Since ϕ is a function of the applied pressure (see Equation 3), Equation 26 represents a transcendental equation for the pressure, p_s.

Buckling of a cylindrical shell in the asymmetric mode is assumed to occur when the applied pressure, p_s, equals the plastic-buckling pressure, p_p. Therefore, the plastic-collapse pressure, p_c, which uniquely defines the plastic-buckling pressure of the shell, is obtained by the simultaneous solution of Equations 22 and 26. As an analytical solution

to these equations would be quite tedious, if not impossible, a graphical solution is recommended. Equation 22 can be plotted in the form p_p versus σ_i and Equation 26 in the form p_s versus σ_i. The intersection of these two curves then defines the collapse pressure, p_c.

Method for Computing Plastic-Collapse Pressure

1. Assume a value for n and compute k and λ by Equation 9. The value of m which will yield a minimum p_c is unity.
2. Calculate coefficients A_1, A_2, A_3, A_4, A_5, A_6, A_7, A_8, and A_9 by Equations 23.
3. Compute E, and E_t and E_s by Equations 19 and 20 for stresses, σ_i, beyond the elastic limit.
4. Assume a value for p_p at a specific σ_i and compute ϕ by Equation 4.
5. Compute p_p by Equation 22.
6. Repeat Steps 4 and 5 until the assumed value of p_p in Step 4 is sufficiently close to the computed value of Step 5.
7. Repeat Steps 1, 2, 4, 5, and 6 varying n at one point on the stress-strain curve to determine the value of n which will yield a minimum p_p.
8. With the value of n thus obtained, repeat Steps 4, 5, and 6 for various values of σ_i between the elastic limit and yield point.

9. Plot p_p versus σ_i in the $p - \sigma_i$ plane.
10. Assume a value for p_s at a specific σ_i and compute ϕ by Equation 4.
11. Compute p_s by Equation 26.
12. Iterate Steps 10 and 11 until the computed p_s equals the assumed p_s.
13. Repeat Steps 10, 11, and 12 for various values of σ_i beyond the elastic limit.
14. Plot p_s versus σ_i in the $p - \sigma_i$ plane.
15. The intersection of the two curves of Steps 9 and 14 gives the collapse pressure, p_c.

The above procedure, outlined for a strain-hardening material, is greatly simplified for an elastic-perfectly plastic material. As the value of σ_i for an elastic-perfectly plastic material is never greater than σ_y, a curve of σ_i versus ϵ_i is a horizontal line in the plastic region, and a plot of p_p versus σ_i in Step 9 is the vertical line $\sigma_i = \sigma_y$.

Elastic-Buckling Theory

When the geometry of the shell structure is such that elastic buckling can occur, the intersection of p_p versus σ_i and p_s versus σ_i occurs for a value of σ_i less than σ_e, the elastic limit of the material. In this case one sees that $E_t/E_s = 1$ and Equation 22 reduces to Reynolds' solution [(3), p. 5] for the elastic-buckling pressure, p_e, which can

be written as follows:

$$p_e = \frac{Eh}{R}\left[\frac{\frac{h^2(k^2+\lambda^2)^2}{12(1-\nu_e^2)} + \frac{\lambda^4}{R^2(k^2+\lambda^2)^2}}{\frac{\lambda^2}{2} + k^2\phi}\right] \qquad [27]$$

A plot of p_e versus σ_i is the horizontal line $p = p_e$ in the $p - \sigma_i$ plane and, therefore, the critical buckling pressure may be obtained directly from Equation 27. Equation 27 is also a transcendental equation, and the elastic-collapse pressure, p_e, must be determined by iteration.

Theoretical Results

Calculations have been carried out for a series of geometries in the plastic-buckling range to show the effect of frame size on the shell-buckling pressure, p_c, according to the developed theory. A strain-hardening steel with a yield strength of 88,000 psi is used for demonstration purposes, and the results are presented in graphical form in Figure 2. As shown in the graph, the flexibility parameter, θ, has a limiting value of 4.0, for which an increase of the relative frame size will not produce any increase in collapse pressure. Thus, at this limit the ratio of frame area to shell area need only be sufficient to prevent frame failure together with shell failure. As θ is a function of h and R and is directly proportional to the bay length, L, it is seen that for a constant h and R, θ is totally dependent on L. For

this case, frame spacing is an important aspect on the effect of frame size. The collapse pressures represented in Figure 2 are for an asymmetric collapse, and thus, for small values of the ratio of frame area to shell area (close to zero) the theory no longer applies, since collapse by general instability would occur.

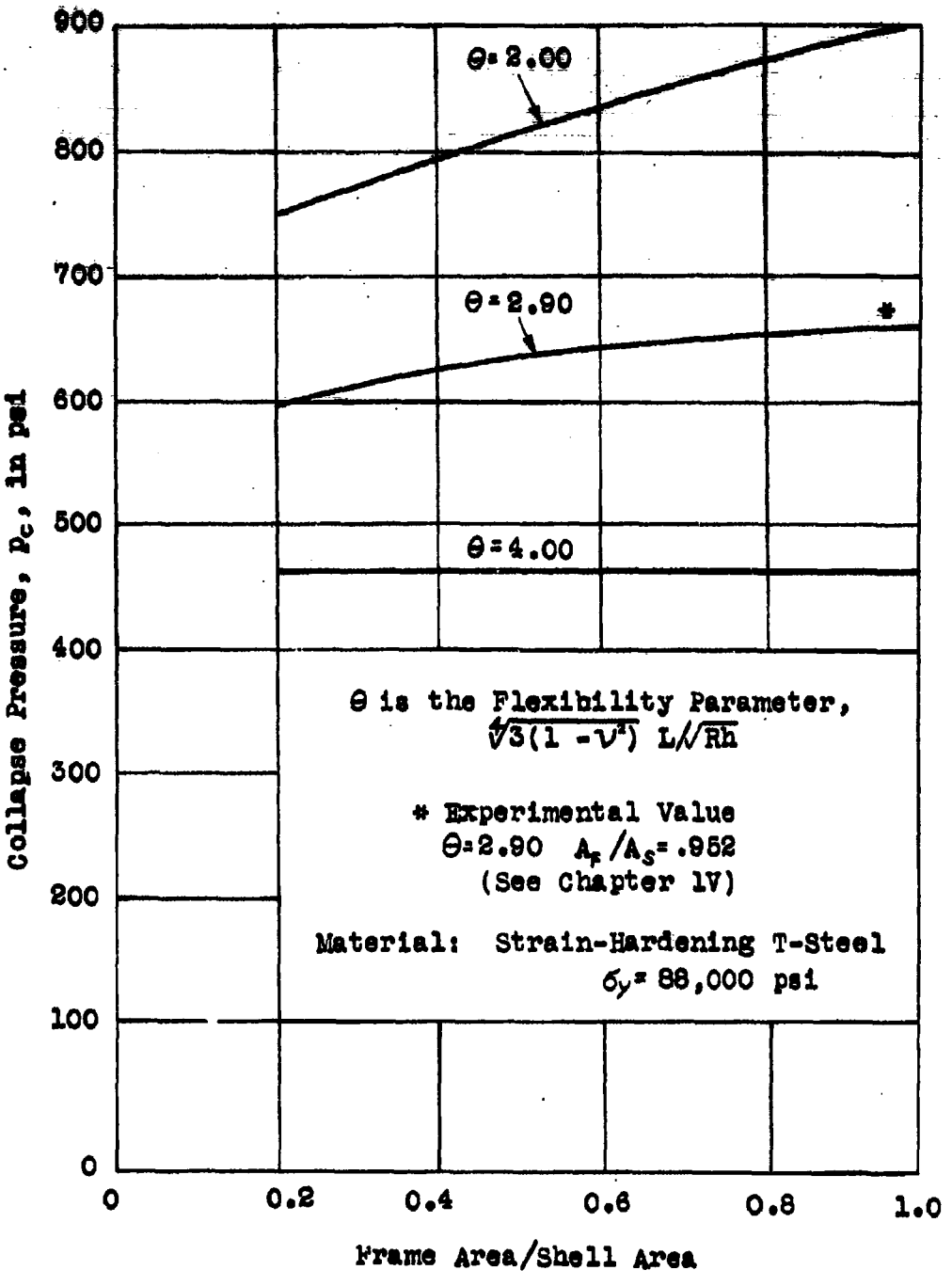

Figure 2 - Effect of Frame Size on Shell-Buckling Pressures of Steel Cylinders

CHAPTER II

EXPERIMENTAL INVESTIGATION

Description of Models

To determine experimentally what effect the circular frames have on a cylindrical shell loaded under external hydrostatic pressure, four models were fabricated and tested in a pressure tank. As pioneering work is currently being conducted in the use of aluminum for oceanographic research vehicles, a high-strength aluminum alloy was chosen. The four models were constructed of 7075-T6 extruded aluminum 5 1/2-in. diameter round bar stock. Machined structural models were favored as opposed to welded models to eliminate the effects of initial deflections and residual stresses which occur in a welded model. Lunchick and Short (13) and Krenzke (14) have shown that, in welded models, the heating and cooling process occurring when the webs of the frames are welded to the shell causes an initial inward frame deflection for an externally-framed cylinder. On the other hand, an initial outward frame deflection occurs for an internally-framed cylinder. These initial deflections cause residual stresses and beam-column effects which can affect collapse pressures.

Each model had the same shell thickness, radius, and typical bay lengths, and only the cross-sectional area of the frames varied. Figure 3 illustrates the various geometries

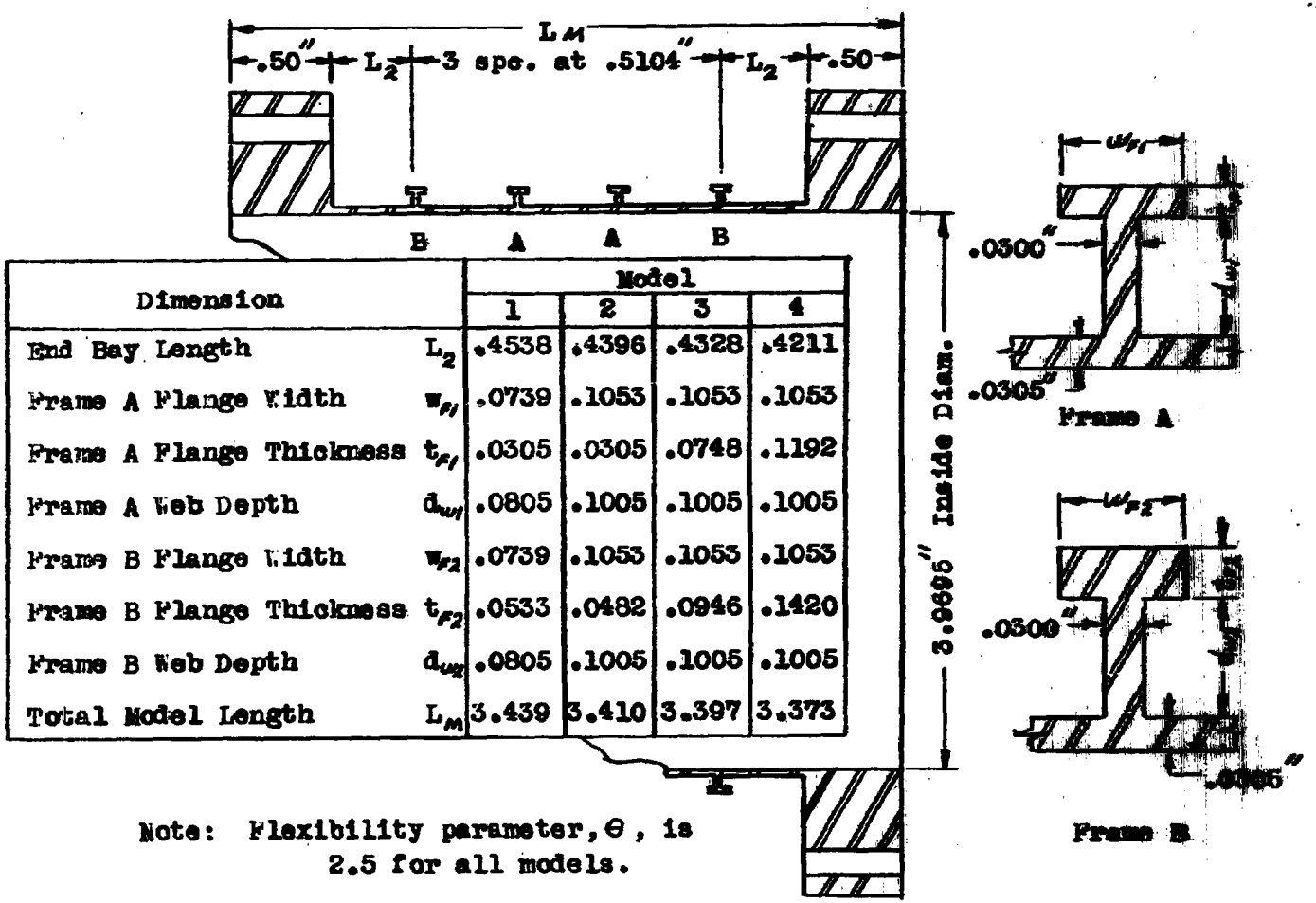

Dimension		Model 1	2	3	4
End Bay Length	L_2	.4538	.4396	.4328	.4211
Frame A Flange Width	w_{f1}	.0739	.1053	.1053	.1053
Frame A Flange Thickness	t_{f1}	.0305	.0305	.0748	.1192
Frame A Web Depth	d_{w1}	.0805	.1005	.1005	.1005
Frame B Flange Width	w_{f2}	.0739	.1053	.1053	.1053
Frame B Flange Thickness	t_{f2}	.0533	.0482	.0946	.1420
Frame B Web Depth	d_{w2}	.0805	.1005	.1005	.1005
Total Model Length	L_M	3.439	3.410	3.397	3.373

Note: Flexibility parameter, θ, is 2.5 for all models.

Figure 3 - Model Cross Section Showing Dimensions

of the models. As is noted, the two end frames of each model have been made larger in cross-sectional area than the two typical frames at midspan, and the lengths of the end bays are slightly changed from that of the three typical bay lengths. These changes are necessary to reduce discontinuity stresses (15) caused by the very rigid closure bulkheads. These end-bay arrangements were designed by the "Optimum End Bay Design" of Short and Bart (16) and, in effect, this design produces a stress distribution in the three center typical bays, which would be the same as that for a circular framed cylinder of infinite length and under external hydrostatic pressure.

Model 1 had a frame area equal to 30 per cent of the shell area. The frame area of Model 2 was 40 per cent of that in the shell. Model 3 had a frame area 70 per cent of the shell, and Model 4, 100 per cent of the shell area. Frame size was varied in the size of the flange and depth of the web. The shape of the frames on all four models was that of a T-section, and the faying width of the webs was held constant in order to hold the bay lengths the same. Dimensions of the frames for each model are noted in tabular form in Figure 3.

Critical dimensions of each model were machined to a tolerance of .0005 in., and were measured after fabrication to check tolerances.

Instrumentation

Models 1 and 3 were instrumented with 38 foil-type electrical resistance strain gages. Fifteen gages were placed

on the inside shell surface of the center bay at midbay in the circumferential direction, equally spaced around a 180-deg. generator. Fifteen additional gages were placed on the outside shell surface directly opposite the inside circumferential midbay gages. Four gages were placed on the inside surface directly beneath the centerline of the typical frames in the circumferential direction, and four gages were placed perpendicular to these for strain measurements in the longitudinal direction.

Models 2 and 4 were instrumented with 34 strain gages. The gages were oriented as in Models 1 and 3, except for the four longitudinal gages utilized on Models 1 and 3 but omitted on Models 2 and 4.

Test Procedure

The tests were conducted in the following order:

1. Model 2
2. Model 4
3. Model 3
4. Model 1

Each model was tested in a pressure tank under external hydrostatic pressure. The ends of the models were closed by a closure bulkhead and each end was sealed by means of an "O" ring. Each model was placed in the pressure tank and a pipeline was connected between the head of the tank and one closure bulkhead, venting the interior of the model to atmospheric pressure. Oil was then poured into the interior of the model to absorb energy expected to be released at the moment

of collapse. The tank head was then sealed, and the model was ready for testing. Figure 4 illustrates the test setup.

Two pressure runs were made on each model. During the first run, strains were recorded at various pressure increments and, when plastic action was observed, the pressure was dropped to zero. Strains were then recorded at zero pressure to determine if any permanent set had occurred. During the second run, strains were also recorded at various pressure increments, but the model was tested to collapse. Table 1 shows the loading schedule and pressure increments at which strains were recorded.

Pressures were applied by means of a hand-operated hydraulic pump and were recorded with a Bourdon-Tube pressure gage. Strains were measured by means of Baldwin Strain Indicators.

Stress-Strain Properties

To apply the plastic-buckling theory, the stress-strain curves of the material had to be accurately determined. Sixteen test specimens were removed from the cylindrical 7075-T6 bar stock. At each end of the bar stock, four specimens were taken in the longitudinal direction and four in the circumferential direction, each at 90-deg. intervals. Each specimen was taken at a 2-in. radius to coincide with the location of the shell of the models. Each specimen was machined into a solid cylinder 1/2 in. in diameter and 2 in. long. Before testing, the diameter of each specimen was

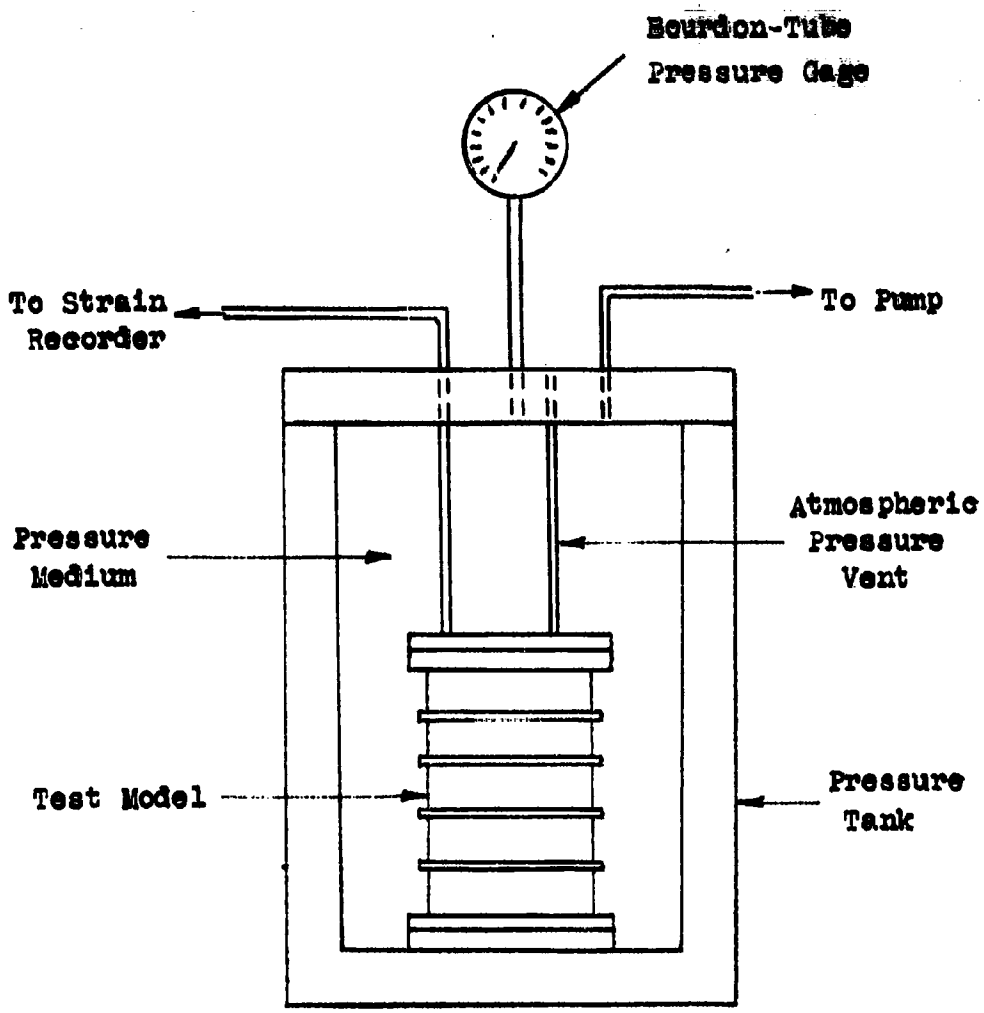

Figure 4 - Test Setup

TABLE 1

LOADING SCHEDULE

Pressure, in psi, At Which Strains Were Recorded							
Model 1		Model 2		Model 3		Model 4	
Run 1	Run 2	Run 1	Run 2	Run 1	Run 2	Run 1	Run 2
0	0	0	0	0	0	0	0
100	250	50	250	200	500	100	500
200	500	100	500	400	750	200	750
300	750	200	750	600	900	300	900
400	900	300	1000	700	1000	400	1000
500	1000	400	1100	800	1100	500	1100
600	1100	500	1200	900	1200	600	1200
700	1200	600	1255	1000#	1300	700	1300
800	1250	700	1300	0	1350	800	1350
900#	1300[a]	800	1355		1400	900	1390[c]
1000	0	900	1375		1420[c]	1000#	0
0		1000#	1400[b]		0	1100	
		1100	0			1200	
		1200				0	
		0					

\# Inelastic action was first observed.

a Failure by general instability occurred before strains could be read.

b Failure by shell buckling occurred before strains could be read.

c Failure by shell yielding occurred before strains could be read.

measured to the nearest 0.0001 in. Each specimen was loaded in compression by a 30,000-lb. testing machine to determine the characteristic load-strain curves. Load-strain curves were obtained on fourteen specimens by means of an automatic recording extensometer, and two circumferential specimens, one from each end of the bar stock, were tested with a Tuckerman strain gage. Elastic limits, together with an assumed yield strength at the 0.2-percent offset of the stress-strain curve, were computed for all sixteen specimens. The elastic, tangent, and secant moduli were computed from results of the Tuckerman tests. Figure 5 illustrates in detail the properties of the 7075-T6 aluminum.

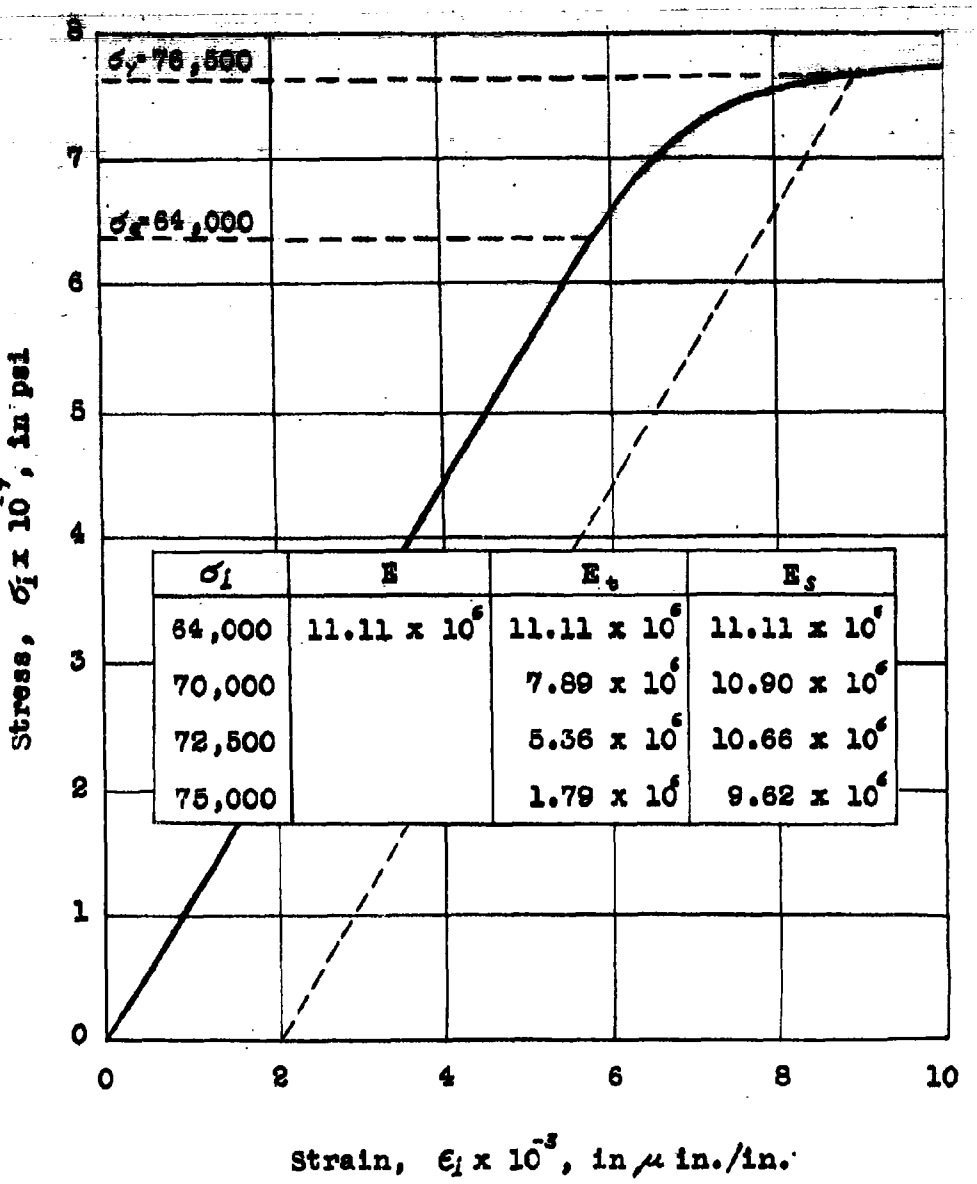

σ_i	E	E_t	E_s
64,000	11.11×10^6	11.11×10^6	11.11×10^6
70,000		7.89×10^6	10.90×10^6
72,500		5.36×10^6	10.66×10^6
75,000		1.79×10^6	9.62×10^6

Figure 5 - Stress-Strain Curve for 7075-T6 Aluminum

CHAPTER III

TEST RESULTS

Model 1, which had a cross-sectional frame area 30 per cent of the shell area, collapsed at a pressure of 1300 psi by plastic general instability. The frames were not of sufficient size to prevent frame failure, and both frames and shell failed simultaneously over the entire length of the model in a single "deep dish" lobe. Width of the lobe was approximately one-eighth of the circumference of the model. Tearing of the shell from the end rings and frames occurred throughout the lobe, and the two center frames buckled inward (see Figure 6). Tearing of the model was a secondary effect, and occurred after collapse because of the brittleness of aluminum.

Model 2, which had a cross-sectional frame area 40 per cent of the shell area, collapsed at 1400 psi by plastic asymmetric buckling. Failure occurred in all three typical bays by a series of nonsymmetrical lobes accompanied by lateral twisting of the frames. The length of the lobes was approximately one-tenth of the circumference of the model. In several places tearing occurred at the shell-frame junctures, but this was not as pronounced as in Model 1. It was observed in areas where tearing did occur, however, that several lobes ran together, giving the appearance of a longer than normal lobe (see Figure 7).

Model 3, which had a cross-sectional frame area 70 per cent of the shell area, collapsed at 1420 psi by axisymmetric shell yielding. Failure occurred in the first typical bay from the end ring along a 180-deg. generator around the circumference. Tearing occurred at the two frame-shell junctures and at midbay (see Figure 8).

Model 4, which had a cross-sectional frame area 100 per cent of the shell area, collapsed at 1390 psi by axisymmetric shell yielding similar to Model 3; however, the area of collapse was more pronounced in Model 4. The length of the failure in Model 4 extended over approximately 200 degrees. Failure occurred in the first typical bay from the end ring and tearing of the shell at the hinge locations occurred as in Model 3 (see Figure 9).

A graphical representation of the collapse pressures is shown in Figure 10, together with various corresponding theoretical formulae. The Hencky-Mises (17) yield criterion at outside midbay assumes that failure occurs when the effective stress, σ_i, on an outside fiber at midbay reaches the yield strength of the material. An extension of this theory is that of Kempner and Salerno (18), in which failure is assumed to occur when the stresses inside at the frame, followed by stresses at outside midbay, reach the yield strength. Lunchick's (4) plastic-hinge theory for axisymmetric collapse is for an elastic-perfectly plastic material and allows for an amount of plastic reserve strength before failure occurs.

Strain data indicated that all models failed in the plastic region. Slight permanent set occurred after the first pressure run, and much more was observed after the models failed. Strain sensitivities for Models 1, 2, 3, and 4 measured during tests are shown in Figure 11, together with the corresponding theoretical strain sensitivities as determined by the Salerno-Pulos (7) theory. Strain levels decreased in the circumferential direction both inside and outside in all four models for an increase of per cent area of frame. However, strain levels increased in the longitudinal direction on the inside surface at the frame for an increase of per cent area of frame.

Fig. 6a Outside View

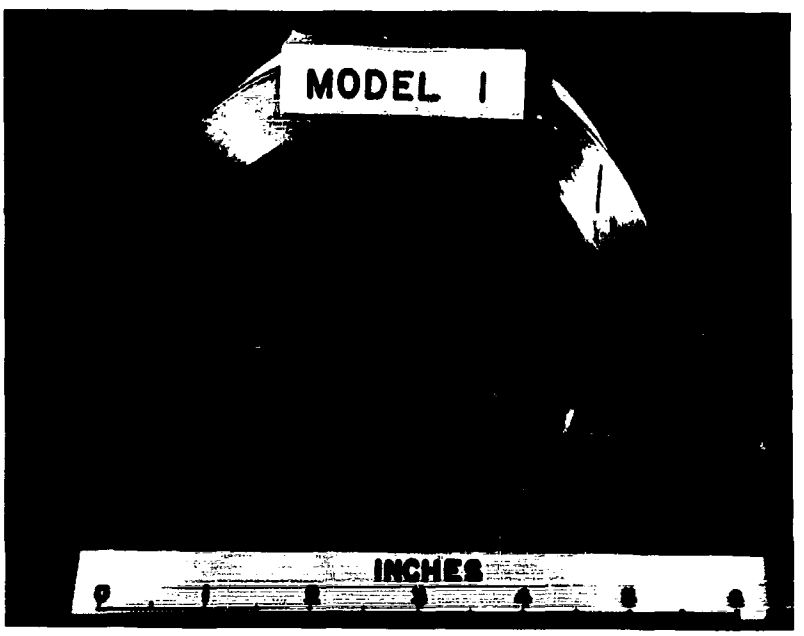

Fig. 6b Inside View

Figure 6 - Model 1 After Collapse

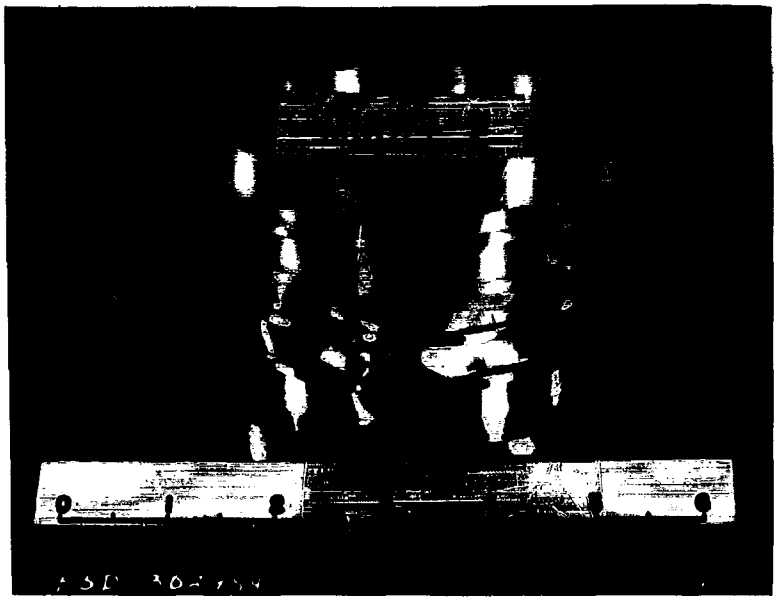

Fig. 7a Outside View

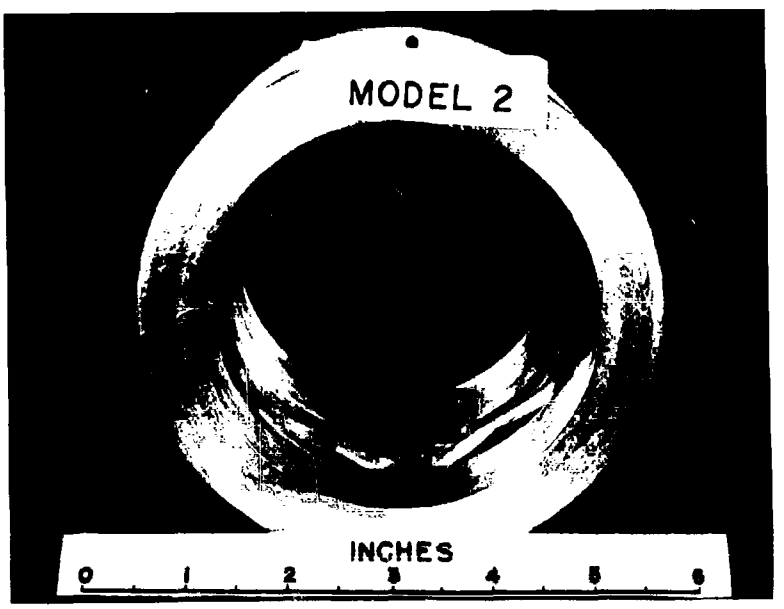

Fig. 7b Inside View

Figure 7 - Model 2 After Collapse

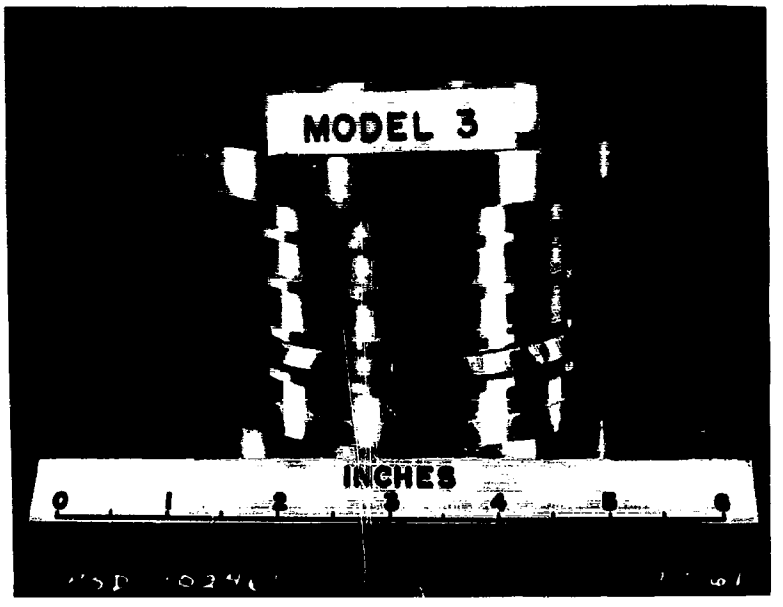

Fig. 8a Outside View

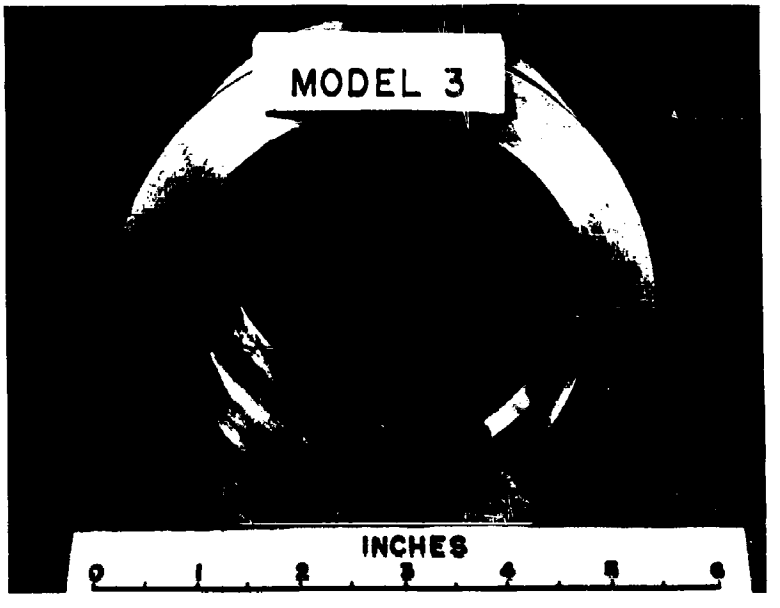

Fig. 8b Inside View

Figure 8 - Model 3 After Collapse

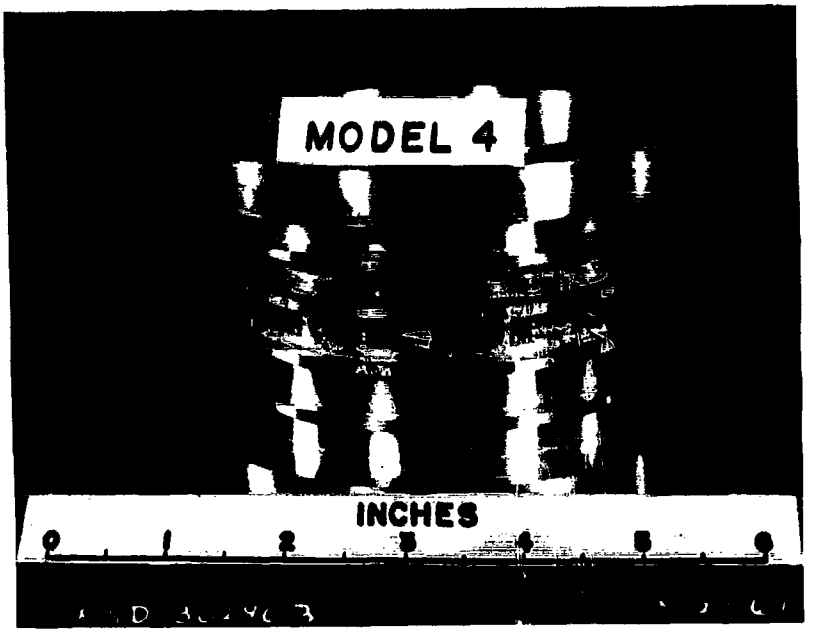

Fig. 9a Outside View

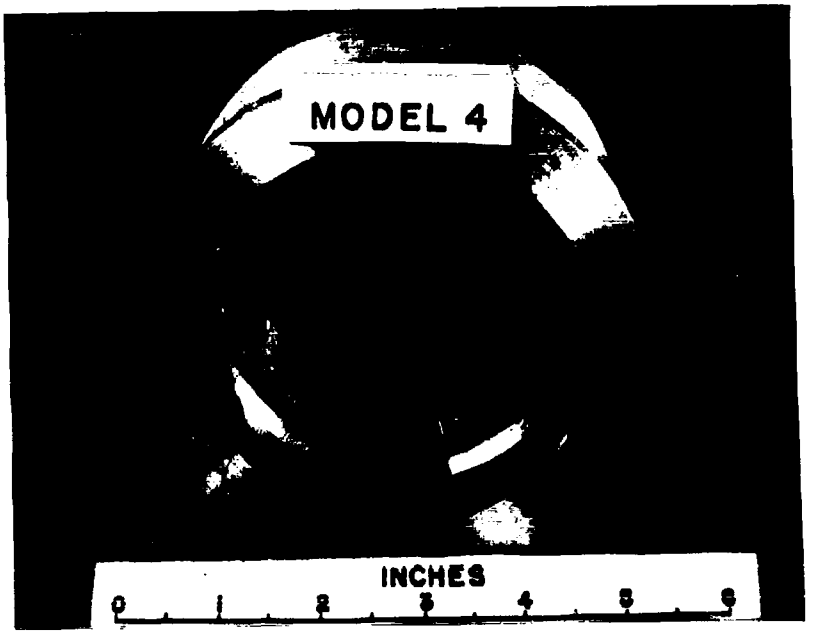

Fig. 9b Inside View

Figure 9 - Model 4 After Collapse

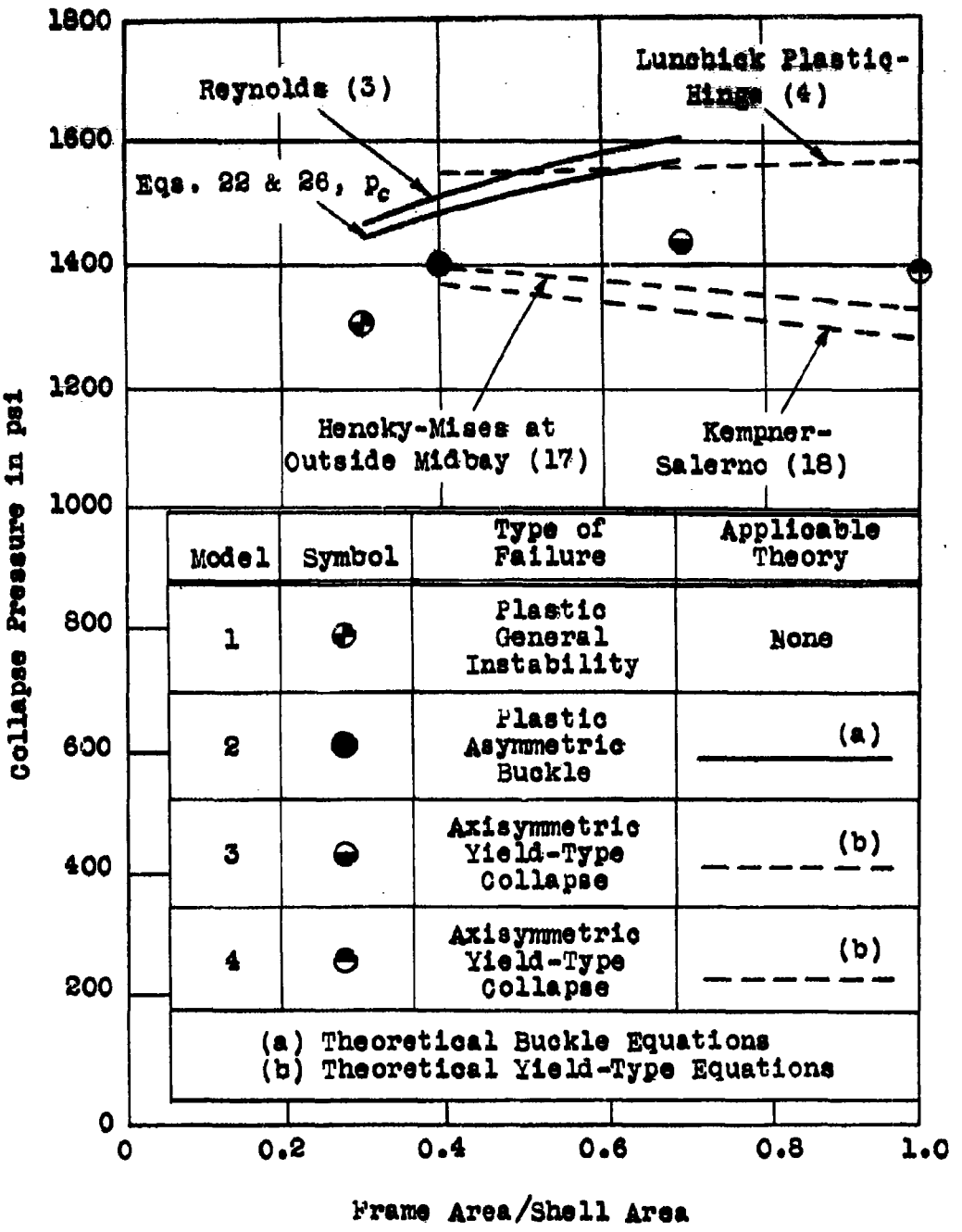

Figure 10 - Effect of Frame Size on Collapse Pressures of Aluminum Cylinders

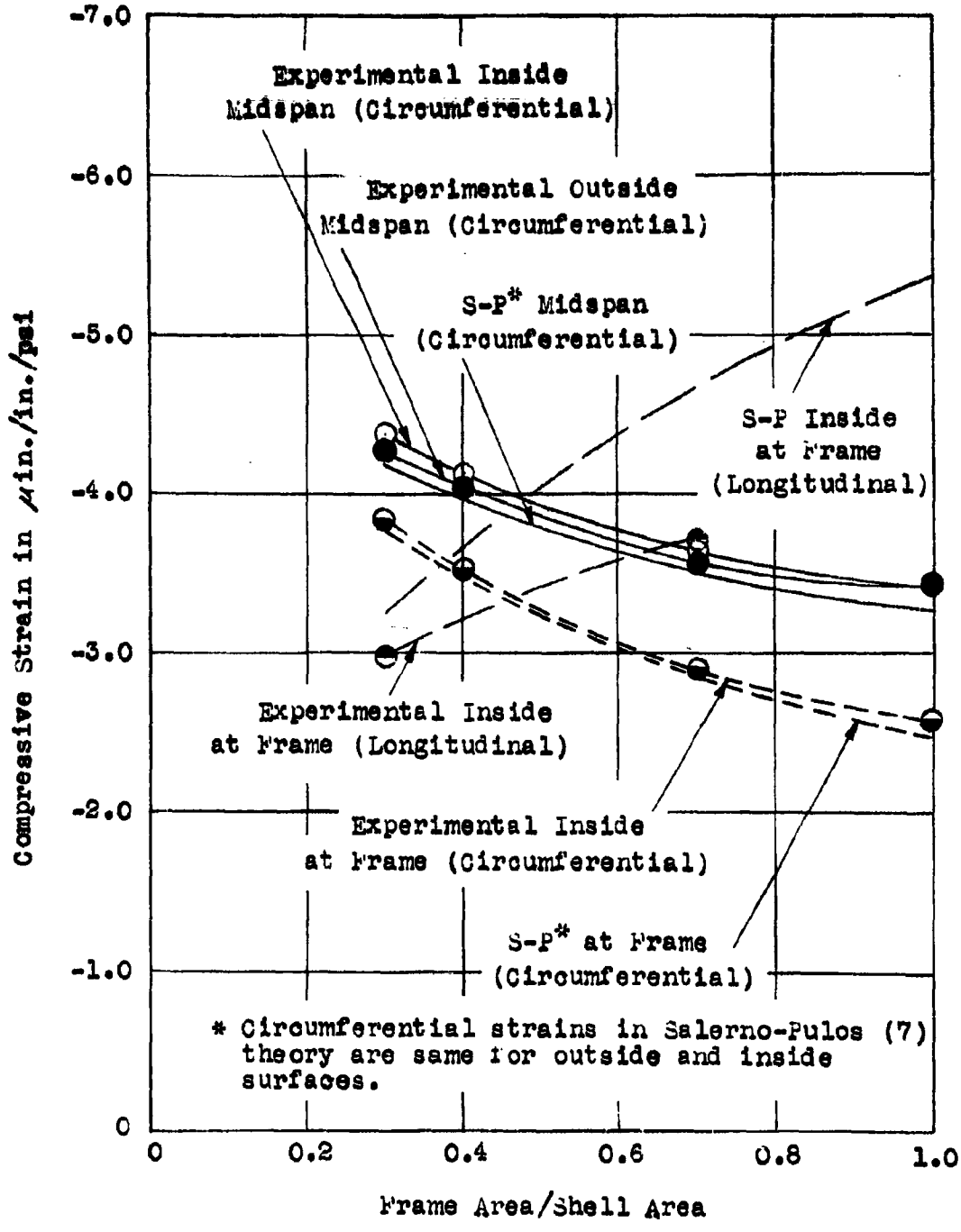

Figure 11 - Effect of Frame Size on Axisymmetric Strains of Aluminum Cylinders

CHAPTER IV

DISCUSSION

Discussion of Experimental Results

The experimental results showed that an appreciable increase in collapse pressure occurred from the 30-percent frame area case to the 40-percent frame area case. This kind of behavior can be explained. At the 30-percent frame area a general instability failure occurred. At the 40-percent frame area buckling of the shell occurred between frames. Only a small increase in collapse pressure occurred between 40-percent and 70-percent frame size. At 70-percent frame size an axisymmetric yield-type failure occurred instead of asymmetric buckling. Strains at the frame indicated that longitudinal stresses grow with an increase of per cent frame size (see Figure 11) which could cause premature yielding. A subsequent increase to 100-percent frame size caused collapse at a lower pressure than that of the 40-percent frame size. For an increase in per cent frame size, the relative decrease in circumferential strains at a frame was greater than the decrease in circumferential strains at midbay. This shows that large frames lower frame deflections, but increase bending of the shell at the frames, thus causing relatively higher longitudinal

stresses in the shell at the frame locations. Therefore, in the case of the 100-percent frame size, the bending stresses in the shell at the frames could have adversely affected the collapse pressure.

Comparison of Theory with Experiment

For the models tested, the asymmetric theory predicts an increase in shell-buckling pressure for an increase in frame size. As only Model 2 failed in this mode, it is difficult to make a positive conclusion concerning the actual trend. However, it would seem reasonable to assume, from the much lower collapse pressure of Model 1 and the higher pressure of Model 3, that the experimental buckling pressures also increase with an increase of frame size to a point where axisymmetric collapse occurs. This increase in buckling pressure for an increase of frame size agrees with Equations 22 and 26, p_c, as shown in Figure 10. Using Equations 22 and 26, p_c, and Lunchick's (4) plastic-hinge theory for axisymmetric collapse, the transition between asymmetric and axisymmetric collapse occurs for a frame area 62 per cent of the shell area, which case is between Models 2 and 3.

The solution of Equations 22 and 26 of this report, Reynolds' (3) theory, and Lunchick's (4) plastic-hinge theory all predict collapse pressures on the unconservative side of the experimental values. Reynolds (3) does not completely account for actual prebuckling stresses in the shell as influenced by the frames, and the plastic-hinge theory is not strictly applicable to a strain-hardening material.

When the Henoky-Mises (17) yield criterion is utilized at outside midbay, theoretical collapse pressures are on the conservative side of the experimental values. The theory of Kempner and Salerno (18) shows collapse pressures slightly lower than those given by the theory of Hencky and Mises (17). The theory of Kempner and Salerno (18) predicts collapse to occur when the effective stresses in the shell on the inside surface at the frame, followed by stresses at outside midbay, reach the yield strength of the material.

The experimental results for aluminum indicate that failure occurs at a point somewhere between the membrane and outer-fiber stress criteria. This should only apply to the aluminum used in these tests, and possibly for other structural materials with the same properties as 7075-T6 aluminum.

The over-all effect of frame size between frames with an area 40 per cent and 100 per cent of the shell area is shown by Lunchick's (4) plastic-hinge theory, which indicates only a slight change in collapse pressure with an increase in frame area. Once axisymmetric yielding occurs, it appears evident that any positive effect of an increase in frame size in increasing collapse pressures is offset by higher bending stresses created both at the frame location and at midbay.

As the test data presented in this report is insufficient for an adequate comparison with the theoretical concepts presented in Chapter I, other experimental data are studied. Reynolds (3), in his comprehensive study of plastic buckling,

also reported the test results of seven steel models, five of welded construction and two machined. Results of these tests are compared with theoretical formulae in Table 2. Equations 22 and 26, p_c, are within an average of 1.9 per cent on the conservative side of test results, the maximum deviation being 3.5 per cent for welded steel construction; average deviation for machined steel construction is 4.9 per cent on the conservative side, the maximum being 6.0 per cent. Model 2 of machined aluminum construction shows a theoretical value 6.1 per cent on the unconservative side of experiment.

Table 2 also shows a comparison between the analysis presented in this report and Reynolds' (3) theoretical results. For the eight geometries considered, Equations 22 and 26, p_c, and Equation 27, p_e, for the plastic- and elastic-buckling pressures, respectively, are approximately 3 per cent on the conservative side of Reynolds' (3) comparable solutions. Figure 12 gives a graphical representation of theoretical versus experimental collapse pressures for the steel cylinders shown in Table 2. Equations 22 and 26, p_c, and Reynolds' (3) plastic equations are shown to agree within approximately 6 per cent of the experiments. The elastic equations, Equation 27, p_e, Mises (1), Sanden and Tölke (2), and Reynolds (3), predict collapse pressures which are unconservative when compared with the experimental results. This can be expected, since all the test models collapsed plastically.

The property parameter, defined as

$$\xi = \frac{h/R}{\sigma_y/E}, \qquad [28]$$

is shown superimposed on the graphs in Figure 12. When h/R is relatively high and σ_y/E is relatively small, a high value of ξ is obtained. This is the case for Model U-12, in which h/R is 0.0193 and σ_y/E is 2.27×10^{-3} for 0.488 frame area to shell area ratio (see Table 2). Also, for small values of h/R and large σ_y/E a low ξ is obtained, as shown for Models T-2A and T-3. The trend of the ξ curve in Figure 12 agrees favorably with the trend of the elastic-buckling equations. This should be expected, as for Model U-12 the large h/R increases the theoretical elastic-buckling pressure, and the small σ_y/E lowers the experimental collapse pressure. Thus, for this case, a high ratio of theoretical collapse to experimental collapse is obtained. Conversely, for Models T-2A and T-3 the small h/R and large σ_y/E produce more conservative values for the ratio of theoretical collapse to experimental collapse. The trend of the plastic-buckling equations is inverted from the ξ curve. This is explained by noting that Equation 22, which defines the plastic-buckling pressure, is a function of the effective stress, σ_1, in the elastic-plastic region. For relatively small values of σ_y/E the effective stresses are also relatively small, and the intersection of Equations 22 and 26 occurs at a relatively lower pressure.

TABLE 2

COMPARISON OF THEORETICAL AND EXPERIMENTAL COLLAPSE PRESSURES

Model Number		T - 2*	T - 3*	T- 6*	T - 2A*	T - 7A*	U - 12*	U - 22*	2
Relative Frame Size**		0.952	0.694	0.609	0.418	0.289	0.488	0.576	0.400
$\sigma_y/E \times 10^3$		2.93	3.60	3.83	3.43	2.80	2.27	2.35	6.89
$h/R \times 10^2$		0.679	0.669	0.953	0.653	0.979	1.093	0.873	1.525
Shape of Frame		Tee					Rectangular		Tee
Material		T - Steel					Mild Steel		7075-T6
Construction		Welded					Machined		
Exp. Collapse Press.		670	553	1005	680	770	975	735	1400
Inelastic Buckling	Eqs. 22 & 26, p_c	662	548	980	691	743	917	707	1485
	T / E***	0.988	0.991	0.975	1.016	0.965	0.940	0.962	1.061
	Reynolds(3)	696	563	1016	705	748	938	734	1502
	T / E	1.039	1.018	1.011	1.037	0.971	0.962	0.999	1.073
Elastic Buckling	Eq. 27, p_e	878	603	1210	755	978	1895	988	1943
	T / E	1.310	1.090	1.204	1.110	1.270	1.944	1.344	1.388
	Reynolds (3)	906	626	1259	756	1010	1907	1002	1976
	T / E	1.352	1.132	1.253	1.112	1.312	1.956	1.362	1.411
	Sanden-Tölke (2)	930	631	1258	773	1032	2014	1054	1977
	T / E	1.388	1.141	1.252	1.137	1.340	2.066	1.434	1.412
	Mises (1)	786	585	1180	705	995	1786	963	1815
	T / E	1.173	1.058	1.174	1.037	1.292	1.832	1.310	1.296

* Data taken from reference 3
** Relative Frame Size is Frame Area/Shell Area
*** Theoretical Collapse/Experimental Collapse

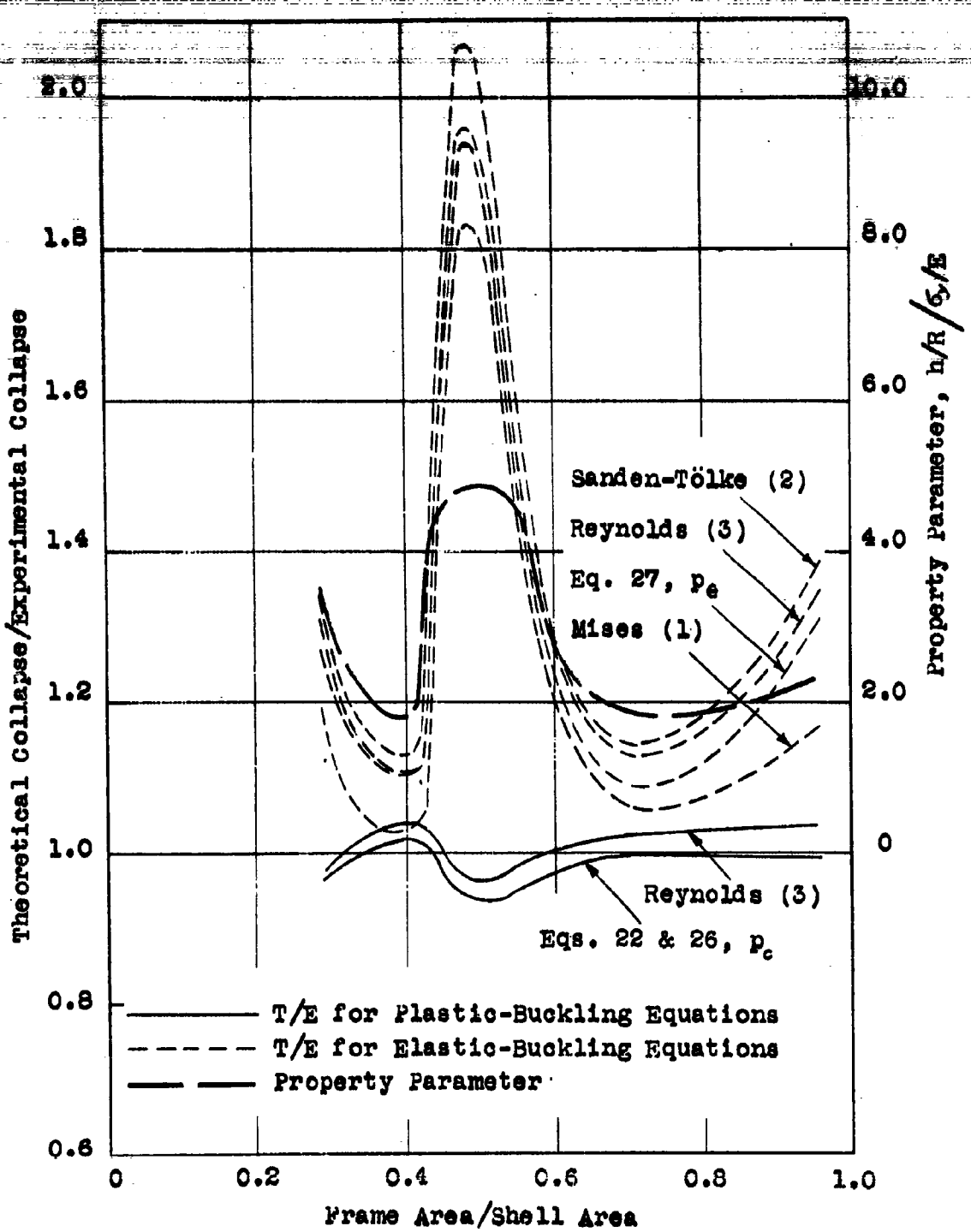

Figure 12 - Graphical Comparison of Theoretical vs Experimental Collapse Pressures for Steel Cylinders

Conclusions

The following conclusions can be made for stiffened cylindrical shells loaded under external hydrostatic pressure:

1. The theory presented by the author for asymmetric buckling adequately predicts collapse pressures for shell geometries constructed from
   a. high-strength steel (Reynolds' (3) experimental data) and
   b. high-strength aluminum,

   when the observed collapse is in the asymmetric mode.

2. For a cylinder made of 7075-T6 aluminum and having a shell flexibility parameter of 2.5, an increase in relative frame size leads to
   a. a change in the observed mode of failure between 30-percent and 40-percent frame size from plastic general instability to plastic asymmetric buckling,
   b. a change in the observed mode of failure between 40-percent and 70-percent frame size from plastic buckling to an axisymmetric yield-type collapse,
   c. a change in the predicted mode of failure from asymmetric buckling to axisymmetric

yielding at 62-percent frame size (Lunchick's (4) plastic hinge and Equations 22 and 26, p_c),

d. an increase in the theoretical asymmetric buckling pressures between 30-percent and 70-percent frame size,

e. an increase in the experimental and theoretical longitudinal bending strains at the frame locations, and

f. a decrease in the experimental and theoretical circumferential strains at the midbay and frame locations.

3. A decrease in the shell flexibility parameter, θ, leads to

   a. an increase in the plastic asymmetric buckling pressures, p_c, for a specified per cent frame size and

   b. a higher rate of increase in the plastic buckling pressures for an increase in per-cent frame size.

ACKNOWLEDGMENTS

This thesis was written under the supervision of Professor R.A. Hechtman of The George Washington University, and is based on a study carried out at the David Taylor Model Basin under the direction of Mr. J. G. Pulos and Dr. M. E. Lunchick. The author wishes to express his gratitude to these individuals for their assistance and suggestions. He is also grateful to Mr. T. E. Reynolds for his valuable comments, and to Mr. R. D. Short for checking the theoretical derivations.

NOTATION

A_F	Effective area of frame cross section, sq. in.
A_i	Coefficients for plastic-buckling equation, $in.^{-s}$
b	Faying width of frame, in.
C_{ii}	Gerard's plasticity coefficients, dimensionless
D	Bending rigidity of shell, $E_s h^3/12(1-\nu^2)$, lb.-in.
E	Young's modulus, psi
E_s	Secant modulus, psi
E_t	Tangent modulus, psi
h	Shell thickness, in.
k	Mode shape coefficient, n/R, $in.^{-1}$
L_F	Center to center spacing of frames, in.
L	Unsupported length of cylinder, L_F - b, in.
M	Moduli parameter, $1 - E_t/E_s$, dimensionless
m, n	Numbers of half-waves of the buckling configuration in axial and circumferential directions, respectively, dimensionless
N_x, N_s, N_{xs}	Forces per unit length, lbs. per in.
p	Pressure, psi
p_e	Elastic buckling pressure, psi
p_p	Plastic buckling pressure, Equation 22, psi
p_c	Plastic collapse pressure, Equations 22 and 26, psi
R	Radius of cylinder to midplane of shell, in.
R_F	Radius of cylinder to c.g. of frame, in.

u, v, w	Shell displacements, in.
x, y, z	Coordinates, dimensionless
α	Effective stress parameter, $3/\sigma_i^2(1 - E_t/E_s)$, psi^{-2}
γ_i	Measure of beam-column effect, $p/2E(R/h)^2\sqrt{1 - \nu^2}$, dimensionless
ξ	Property parameter, $\frac{h/R}{\sigma_y/E}$, dimensionless
γ	Shear strain, radians
ϵ_x, ϵ_s	Membrane strains, in. per in.
ϵ_i	Effective strain, in. per in.
θ	Shell flexibility parameter, $[3(1 - \nu^2)]^{1/4} L/\sqrt{Rh}$, dimensionless
λ	Mode shape coefficient, $m\pi/L$, $in.^{-1}$
ν	Poisson's ratio, dimensionless
ν_e	Elastic value of Poisson's ratio, dimensionless
σ_x, σ_s	Membrane stresses, psi
σ_i	Effective stress, psi
σ_e	Elastic limit stress, psi
σ_y	Yield stress, psi
ϕ	Stress function, dimensionless
τ	Shear stress, psi

APPENDIX A

For simplification, the terms F_1 and F_2 in the Salerno-Pulos axisymmetric stress distribution expressions are shown in Figures 13 and 14 where

$$F_1 = \left(\frac{4}{\theta}\right)\left[\frac{\cosh^2\eta_1\theta - \cos^2\eta_2\theta}{\frac{\cosh\eta_1\theta\,\sinh\eta_1\theta}{\eta_1} + \frac{\cos\eta_2\theta\,\sin\eta_2\theta}{\eta_2}}\right] \qquad [A1]$$

$$F_2 = \frac{\frac{\cosh\eta_1\theta\,\sin\eta_2\theta}{\eta_2} + \frac{\sinh\eta_1\theta\,\cos\eta_2\theta}{\eta_1}}{\frac{\cosh\eta_1\theta\,\sinh\eta_1\theta}{\eta_1} + \frac{\cos\eta_2\theta\,\sin\eta_2\theta}{\eta_2}},$$

in which

$$\eta_1 = \frac{1}{2}\sqrt{1-\gamma_1}$$

$$\eta_2 = \frac{1}{2}\sqrt{1+\gamma_1} \qquad [A2]$$

$$\theta = \sqrt[4]{3(1-\nu^2)}\,\frac{L}{\sqrt{Rh}},$$

and

$$\gamma_1 = \frac{p}{2E}\left(\frac{R}{h}\right)^2\sqrt{3(1-\nu^2)}. \qquad [A3]$$

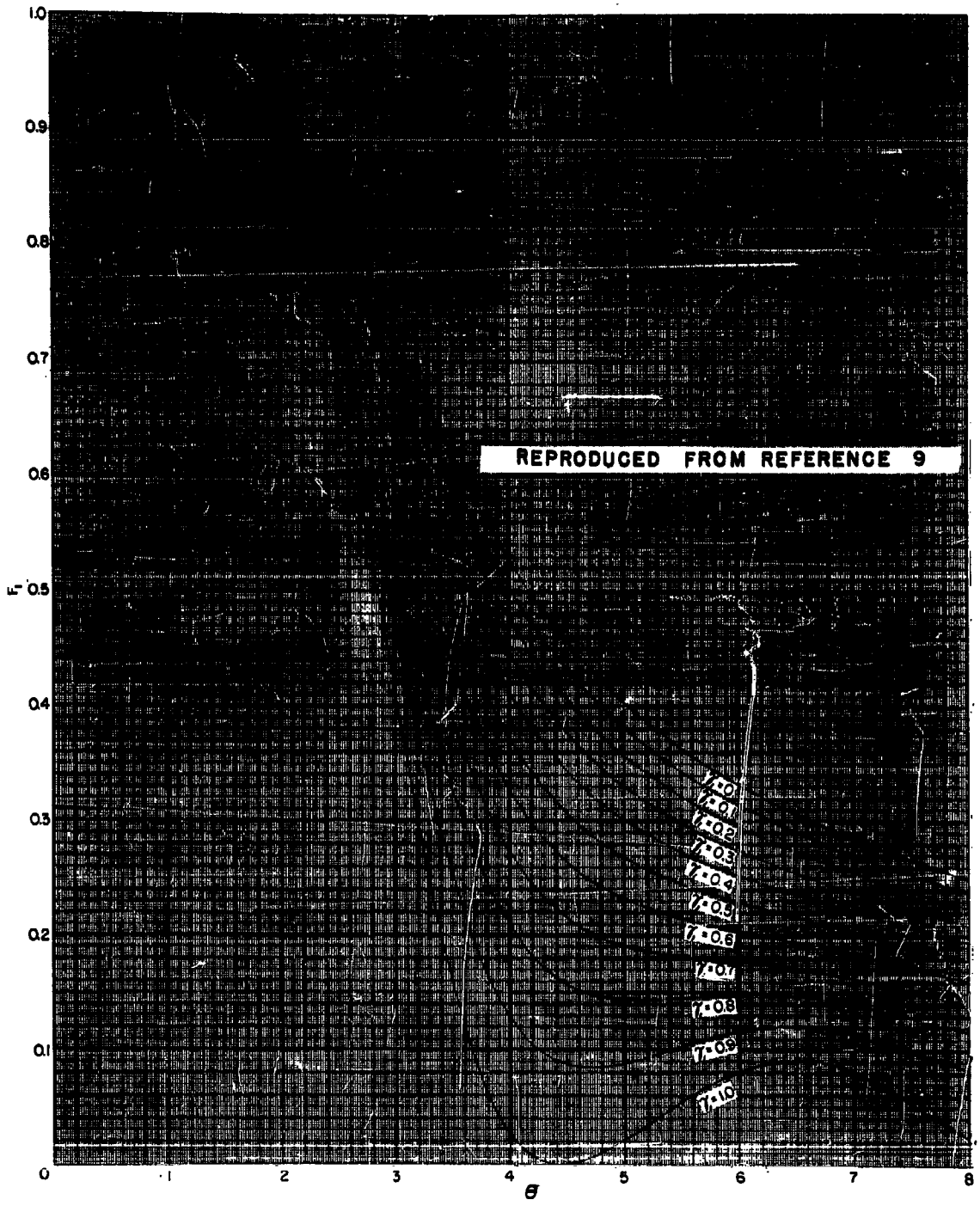

Figure 13 - Function F,

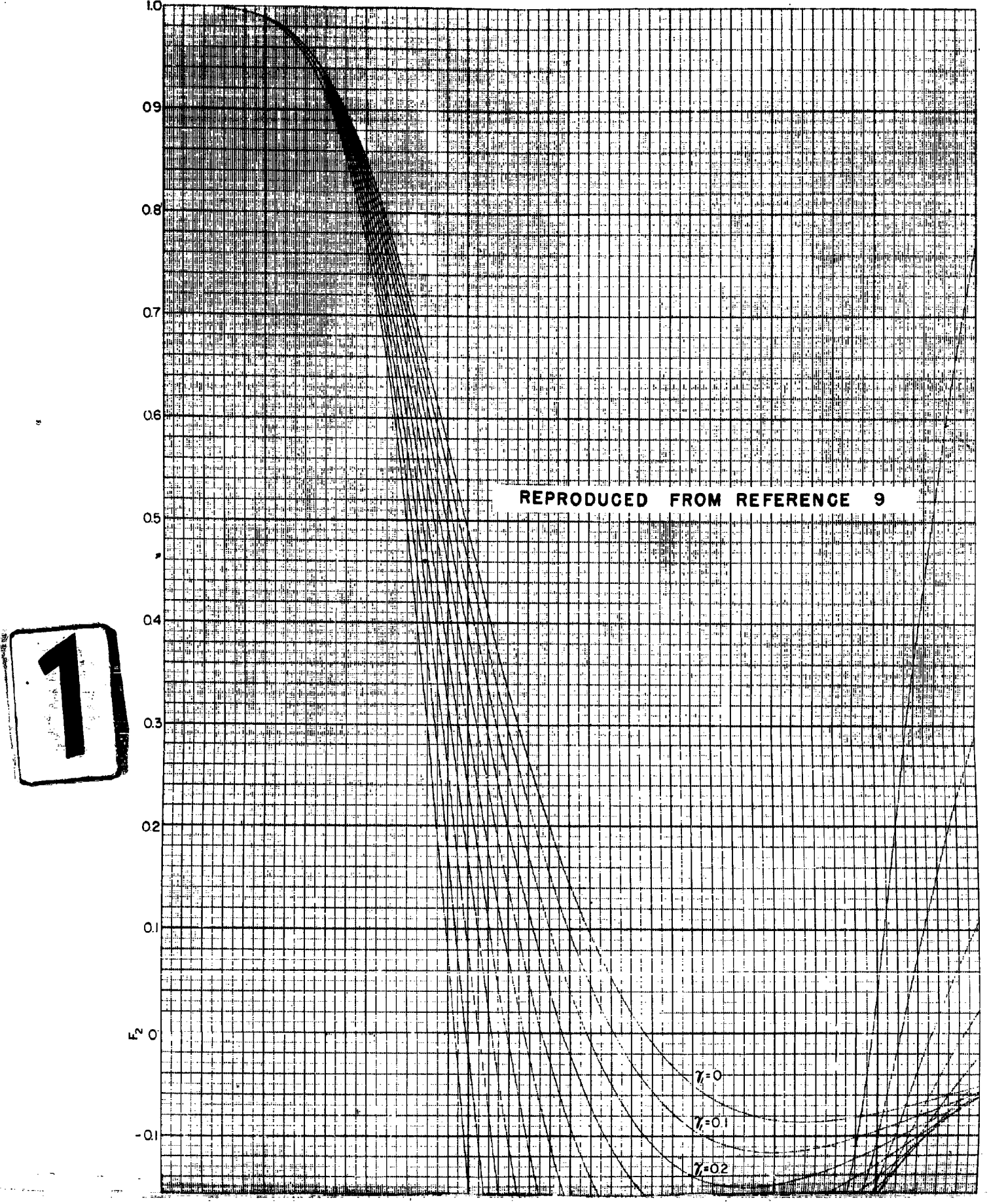
1.0
0.9
0.8
0.7
0.6
0.5
0.4
0.3
0.2
0.1
0
-0.1
F_2
REPRODUCED FROM REFERENCE 9
$\gamma_1 = 0$
$\gamma_1 = 0.1$
$\gamma_1 = 0.2$

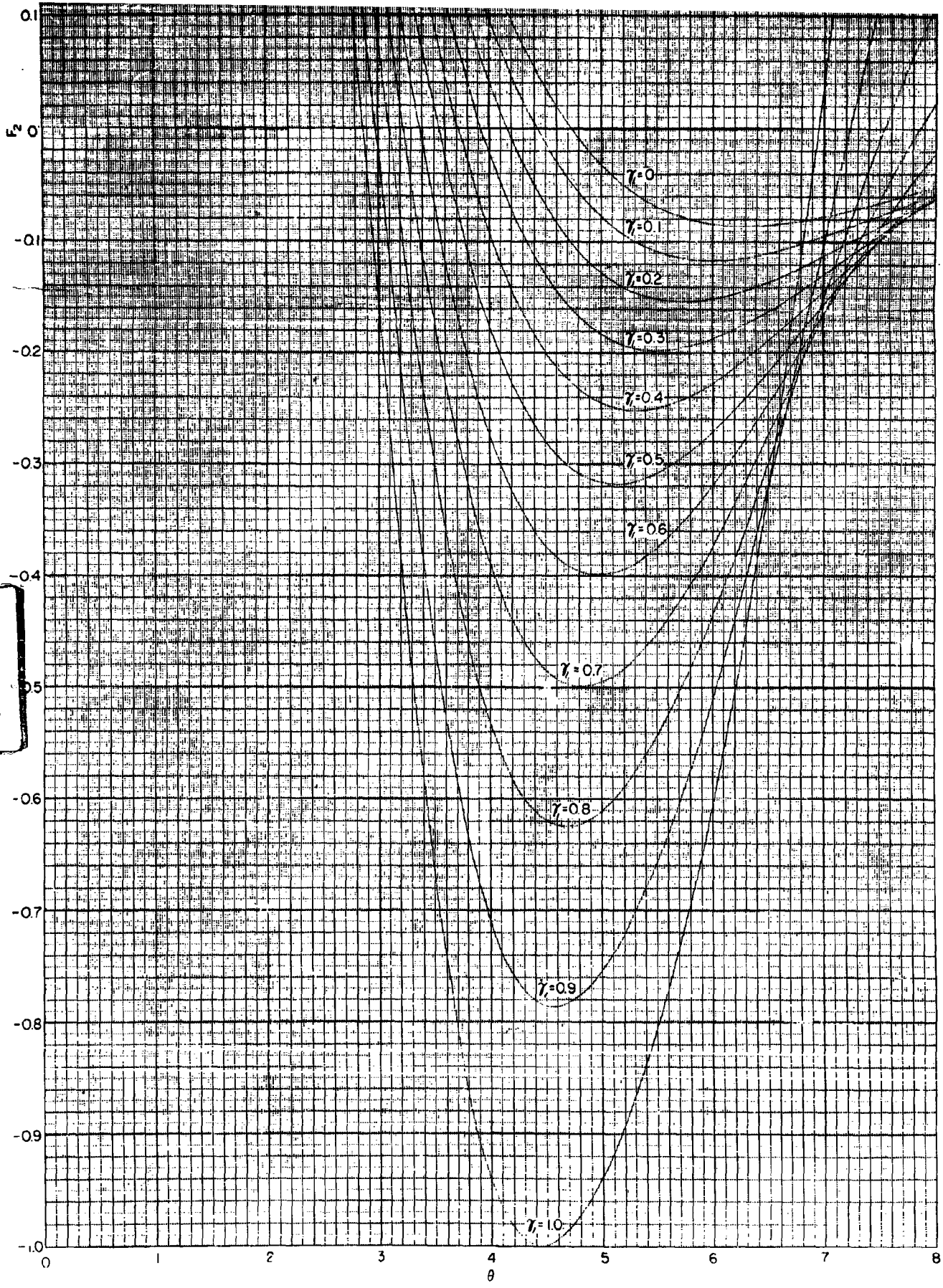

Figure 14 - Function F_2

APPENDIX B

Gerard (6), in his derivation of the plastic-buckling equilibrium equations, assumes that when buckling occurs the displacements u, v, and w increase slightly from that of the displaced equilibrium position just before buckling. These changes in displacements cause incremental changes in the forces and moments, designated by primes, ('), and are defined as follows:

$$N_x' = B\left(C_{11}\epsilon_1 + \tfrac{1}{2}C_{12}\epsilon_2 - \tfrac{1}{2}C_{13}\epsilon_3\right)$$

$$N_s' = B\left(C_{22}\epsilon_2 + \tfrac{1}{2}C_{21}\epsilon_1 - \tfrac{1}{2}C_{23}\epsilon_3\right)$$

$$N_{xs}' = \frac{B}{2}\left(C_{33}\epsilon_3 - \tfrac{1}{2}C_{31}\epsilon_1 - \tfrac{1}{2}C_{32}\epsilon_2\right)$$

$$M_x' = -D\left(C_{11}\chi_1 + \tfrac{1}{2}C_{12}\chi_2 - \tfrac{1}{2}C_{13}\chi_3\right) \qquad [B1]$$

$$M_s' = -D\left(C_{22}\chi_2 + \tfrac{1}{2}C_{21}\chi_1 - \tfrac{1}{2}C_{23}\chi_3\right)$$

$$M_{xs}' = -\frac{D}{2}\left(C_{33}\chi_3 - \tfrac{1}{2}C_{31}\chi_1 - \tfrac{1}{2}C_{32}\chi_2\right),$$

where

$$\epsilon_1 = \frac{\partial u}{\partial x}$$

$$\epsilon_2 = \frac{\partial v}{\partial s} + \frac{w}{R}$$

$$\epsilon_3 = \frac{1}{2}\left(\frac{\partial u}{\partial s} + \frac{\partial v}{\partial x}\right)$$

$$\chi_1 = \frac{\partial^2 w}{\partial x^2} \qquad [B2]$$

$$\chi_2 = \frac{\partial^2 w}{\partial s^2}$$

$$\chi_3 = \frac{\partial^2 w}{\partial x \partial s},$$

and the plasticity coefficients are as follows:

$$C_{11} = 1 - \alpha \frac{\sigma_x^2}{4}$$

$$C_{22} = 1 - \alpha \frac{\sigma_s^2}{4}$$

$$C_{33} = 1 - \alpha \tau^2$$

$$C_{21} = C_{12} = 1 - \alpha \frac{\sigma_x \sigma_s}{2} \qquad [B3]$$

$$C_{31} = C_{13} = \alpha \sigma_x \tau$$

$$C_{32} = C_{23} = \alpha \sigma_s \tau,$$

in which the effective stress parameter is

$$\alpha = \frac{3}{\sigma_i^2}\left(1 - \frac{E_t}{E_s}\right).$$

The axial rigidity is

$$B = \frac{4E_s h}{3} \qquad [B4]$$

and the bending rigidity is

$$D = \frac{E_s h^3}{9}, \qquad [B5]$$

and the effective stress, as defined by the octahedral shear law, is

$$\sigma_i = (\sigma_x^2 + \sigma_s^2 - \sigma_x \sigma_s + 3\tau^2)^{\frac{1}{2}}. \qquad [B6]$$

In the above equations Gerard has made the assumption that Poisson's ratio is 1/2, which is true for an isotropic, incompressible material. This simplifies the derivation of the equilibrium equations.

The equilibrium equations, as shown by Gerard, are

$$\Sigma F_x = \frac{\partial N_x'}{\partial x} + \frac{\partial N_{xs}'}{\partial s} = 0$$

$$\Sigma F_s = \frac{\partial N_s'}{\partial s} + \frac{\partial N_{xs}'}{\partial x} = 0$$

$$\Sigma F_z = -\frac{\partial^2 M_x'}{\partial x^2} - 2\frac{\partial^2 M_{xs}'}{\partial x\, \partial s} - \frac{\partial^2 M_s'}{\partial s^2} + \frac{N_s'}{R} + N_x \frac{\partial^2 w}{\partial x^2} + 2N_{xs}\frac{\partial^2 w}{\partial x\, \partial s} + N_s \frac{\partial^2 w}{\partial s^2} + p = 0 \qquad [B7]$$

where N_x, N_s, and N_{xs} are loads per unit width, and p is external pressure. By use of Equations B1 and B2 these equilibrium equations can be written in terms of the displacements and their derivatives:

$$C_{11}\frac{\partial^2 u}{\partial x^2} - \frac{C_{13}}{2}\frac{\partial^2 u}{\partial x\,\partial s} + \frac{C_{33}}{4}\frac{\partial^2 u}{\partial s^2} - \frac{C_{13}}{4}\frac{\partial^2 v}{\partial x^2}$$
$$+\left(\frac{C_{12}}{2} + \frac{C_{33}}{4}\right)\frac{\partial^2 v}{\partial x\,\partial s} - \frac{C_{23}}{4}\frac{\partial^2 v}{\partial s^2} + \frac{C_{12}}{2R}\frac{\partial w}{\partial x}$$
$$-\frac{C_{23}}{4R}\frac{\partial w}{\partial s} = 0$$

$$C_{22}\frac{\partial^2 v}{\partial s^2} - \frac{C_{23}}{2}\frac{\partial^2 v}{\partial x\,\partial s} + \frac{C_{33}}{4}\frac{\partial^2 v}{\partial x^2} - \frac{C_{13}}{4}\frac{\partial^2 u}{\partial x^2}$$
$$+\left(\frac{C_{12}}{2} + \frac{C_{33}}{4}\right)\frac{\partial^2 u}{\partial x\,\partial s} - \frac{C_{23}}{4}\frac{\partial^2 u}{\partial s^2}$$
$$+\frac{C_{22}}{R}\frac{\partial w}{\partial s} - \frac{C_{23}}{4R}\frac{\partial w}{\partial x} = 0$$

[B8]

$$D\left[C_{11}\frac{\partial^4 w}{\partial x^4} - C_{13}\frac{\partial^4 w}{\partial x^3\,\partial s} + \left(C_{12} + C_{33}\right)\frac{\partial^4 w}{\partial x^2\,\partial s^2}\right.$$
$$\left. - C_{23}\frac{\partial^4 w}{\partial x\,\partial s^3} + C_{22}\frac{\partial^4 w}{\partial s^4}\right]$$
$$+\frac{B}{R}\left(\frac{C_{12}}{2}\frac{\partial u}{\partial x} - \frac{C_{23}}{4}\frac{\partial u}{\partial s} - \frac{C_{23}}{4}\frac{\partial v}{\partial x}\right.$$
$$\left. + C_{22}\frac{\partial v}{\partial s} + C_{22}\frac{w}{R}\right)$$
$$+N_x\frac{\partial^2 w}{\partial x^2} + 2N_{xs}\frac{\partial^2 w}{\partial x\,\partial s} + N_s\frac{\partial^2 w}{\partial s^2} + p = 0.$$

LIST OF REFERENCES

1. Von Mises, R., The Critical External Pressure of Cylindrical Tubes Under Uniform Radial and Axial Load, Experimental Model Basin Translation 366, August, 1933.

2. Von Sanden, K. and Tölke, F., On Stability Problems in Thin Cylindrical Shells, David Taylor Model Basin Translation 33, December, 1949.

3. Reynolds, T. E., Inelastic Lobar Buckling of Circular Cylindrical Shells Under External Hydrostatic Pressure, David Taylor Model Basin Report 1392, August, 1960.

4. Lunchick, M. E., Ph. D., Yield Failure of Stiffened Cylinders Under Hydrostatic Pressure, David Taylor Model Basin Report 1291, January, 1959.

5. Lunchick, M. E., Ph. D., Plastic Axisymmetric Buckling of Ring-Stiffened Cylindrical Shells Fabricated From Strain-Hardening Materials and Subjected to External Hydrostatic Pressure, David Taylor Model Basin Report 1393, January, 1961.

6. Gerard, G., Compressive and Torsional Buckling of Thin-Wall Cylinders in Yield Region, National Advisory Committee for Aeronautics Note 3726, August, 1956.

7. Salerno, V. L. and Pulos, J. G., Stress Distribution in a Circular Cylindrical Shell Under Hydrostatic Pressure Supported by Equally Spaced Circular Ring Frames, Polytechnic Institute of Brooklyn, Department of Aeronautical Engineering and Applied Mechanics, Report 171-A, June, 1951.

8. Von Sanden, K. and Günther, K., The Strength of Cylindrical Shells, Stiffened by Frames and Bulkheads, Under Uniform External Pressure on All Sides, David Taylor Model Basin Translation 38, March, 1952.

9. Krenzke, M. A. and Short, R. D., Jr., Graphical Method for Determining Stresses in Ring-Stiffened Cylinders Under External Hydrostatic Pressure, David Taylor Model Basin Report 1348, October, 1959.

10. Nadai, A., Theories of Strength, Journal of Applied Mechanics, Vol. I, No. 3, Jul.-Sep., 1933, pp 111-129.

11. Hoffman, O. and Sachs, G., Introduction to the Theory of Plasticity for Engineers, New York, McGraw-Hill Book Co., Inc., 1953, p. 17.

12. Gerard, G. and Wildhorn, S., A Study of Poisson's Ratio in the Yield Region, National Advisory Committee for Aeronautics Technical Note 2561, June, 1952.

13. Lunchick, M. E., Ph. D. and Short, R. D., Jr., Behavior of Cylinders With Initial Shell Deflections, Journal of Applied Mechanics, Vol. 24, No. 4, December 1957, pp. 559-564.

14. Krenzke, M. A., Effect of Initial Deflections and Residual Welding Stresses on Elastic Behavior and Collapse Pressure of Stiffened Cylinders Subjected to External Hydrostatic Pressure, David Taylor Model Basin Report 1327, April, 1960.

15. Timoshenko, S. and Woinowsky-Krieger, S., Theory of Plates and Shells, 2d ed., New York, McGraw-Hill Book Co., Inc., 1959, p. 483.

16. Short, R. D., Jr. and Bart, R., Analysis for Determining Stresses in Stiffened Cylindrical Shells Near Structural Discontinuities, David Taylor Model Basin Report 1065, January, 1959.

17. Seely, F. B. and Smith, J. O., Advanced Mechanics of Materials, New York, John Wiley and Sons, Inc., 1955, p. 81.

18. Kempner, J. and Salerno, V. L., Analysis of Inelastic Behavior of Transversely Reinforced Cylindrical Shells Under Hydrostatic Pressure, Polytechnic Institute of Brooklyn Aeronautical Laboratory Report No. 172, August, 1950.

INITIAL DISTRIBUTION

Copies	
14	CHBUSHIPS
	2 Sci & Res Sec (442)
	1 Lab Mgt (320)
	3 Tech Info Br (335)
	1 Ships Res Br (341A)
	1 Applied Sci Br (342A)
	1 Prelim Des Br (420)
	1 Prelim Des Sec (421)
	1 Ship Protec (423)
	1 Hull Des Br (440)
	1 Struc Sec (443)
	1 Sub Br (525)
1	CHONR (439)
1	CNO (Op 07TB)
1	CDR, USNOL
1	CDR, USNRL (2027)
1	CDR, USNOTS, China Lake
1	CO, USNUOS, Newport
1	CO, USNUSL, New London
10	CDR, ASTIA
2	NAVSHIPYD PTSMH
1	NAVSHIPYD MARE
1	NAVSHIPYD CHASN
1	NAVSHIPYD NY Matl Lab (948)
1	SUPSHIP, Groton
1	Elec Boat Div, Genl Dyn Corp
1	SUPSHIP, Newport News
1	NNSB & DD Co
1	SUPSHIP, Pascagoula
1	Ingalls Shipbldg Corp
1	DIR DEF R & E, attn: Tech Lib
1	CO, USNROTC & NAVADMINU, MIT
1	O in C, PGSCOL, Webb
1	Dr. E. Wenk, Jr., The White House
1	Dr. R.C. De Hart, SW Res Inst
1	Prof. J. Kempner, Polytechn Inst of Bklyn
1	Dean V.L. Salerno, Fairleigh Dickinson Univ
2	Dr. G. Gerard, College of Engin, New York Univ

David Taylor Model Basin. Report 1600.
INVESTIGATION ON THE INFLUENCE OF STIFFENER SIZE ON THE BUCKLING PRESSURES OF CIRCULAR CYLINDRICAL SHELLS UNDER HYDROSTATIC PRESSURE, by James A. Nott. Dec 1961. ii, 63p. illus., graphs, tables, refs. UNCLASSIFIED

A theoretical derivation is given for elastic and plastic buckling of stiffened circular cylindrical shells under external hydrostatic pressure. The theory accounts for variable shell stresses, as influenced by the circular stiffeners, and critical buckling pressures are obtained for simple support conditions at the shell-frame junctures. Methods are given for the determination of collapse pressures for both elastic and plastic asymmetric buckling by iteration and numerical minimization. The theory is applicable to shells made either of strain-hardening or elastic-perfectly plastic materials.

1. Cylindrical shells (Stiffened)--Pressure--Measurement
2. Cylindrical shells (Stiffened)--Buckling--Measurement
3. Cylindrical shells (Stiffened)--Elasticity--Model tests
4. Cylindrical shells (Stiffened)--Failure
I. Nott, James A.
II. S-F013 03 02

David Taylor Model Basin. Report 1600.
INVESTIGATION ON THE INFLUENCE OF STIFFENER SIZE ON THE BUCKLING PRESSURES OF CIRCULAR CYLINDRICAL SHELLS UNDER HYDROSTATIC PRESSURE, by James A. Nott. Dec 1961. ii, 63p. illus., graphs, tables, refs. UNCLASSIFIED

A theoretical derivation is given for elastic and plastic buckling of stiffened circular cylindrical shells under external hydrostatic pressure. The theory accounts for variable shell stresses, as influenced by the circular stiffeners, and critical buckling pressures are obtained for simple support conditions at the shell-frame junctures. Methods are given for the determination of collapse pressures for both elastic and plastic asymmetric buckling by iteration and numerical minimization. The theory is applicable to shells made either of strain-hardening or elastic-perfectly plastic materials.

1. Cylindrical shells (Stiffened)--Pressure--Measurement
2. Cylindrical shells (Stiffened)--Buckling--Measurement
3. Cylindrical shells (Stiffened)--Elasticity--Model tests
4. Cylindrical shells (Stiffened)--Failure
I. Nott, James A.
II. S-F013 03 02

David Taylor Model Basin. Report 1600.
INVESTIGATION ON THE INFLUENCE OF STIFFENER SIZE ON THE BUCKLING PRESSURES OF CIRCULAR CYLINDRICAL SHELLS UNDER HYDROSTATIC PRESSURE, by James A. Nott. Dec 1961. ii, 63p. illus., graphs, tables, refs. UNCLASSIFIED

A theoretical derivation is given for elastic and plastic buckling of stiffened circular cylindrical shells under external hydrostatic pressure. The theory accounts for variable shell stresses, as influenced by the circular stiffeners, and critical buckling pressures are obtained for simple support conditions at the shell-frame junctures. Methods are given for the determination of collapse pressures for both elastic and plastic asymmetric buckling by iteration and numerical minimization. The theory is applicable to shells made either of strain-hardening or elastic-perfectly plastic materials.

1. Cylindrical shells (Stiffened)--Pressure--Measurement
2. Cylindrical shells (Stiffened)--Buckling--Measurement
3. Cylindrical shells (Stiffened)--Elasticity--Model tests
4. Cylindrical shells (Stiffened)--Failure
I. Nott, James A.
II. S-F013 03 02

David Taylor Model Basin. Report 1600.
INVESTIGATION ON THE INFLUENCE OF STIFFENER SIZE ON THE BUCKLING PRESSURES OF CIRCULAR CYLINDRICAL SHELLS UNDER HYDROSTATIC PRESSURE, by James A. Nott. Dec 1961. ii, 63p. illus., graphs, tables, refs. UNCLASSIFIED

A theoretical derivation is given for elastic and plastic buckling of stiffened circular cylindrical shells under external hydrostatic pressure. The theory accounts for variable shell stresses, as influenced by the circular stiffeners, and critical buckling pressures are obtained for simple support conditions at the shell-frame junctures. Methods are given for the determination of collapse pressures for both elastic and plastic asymmetric buckling by iteration and numerical minimization. The theory is applicable to shells made either of strain-hardening or elastic-perfectly plastic materials.

1. Cylindrical shells (Stiffened)--Pressure--Measurement
2. Cylindrical shells (Stiffened)--Buckling--Measurement
3. Cylindrical shells (Stiffened)--Elasticity--Model tests
4. Cylindrical shells (Stiffened)--Failure
I. Nott, James A.
II. S-F013 03 02

Using the theory developed in this report it is shown that a variation in stiffener size can change the buckling pressures. Test data from high-strength steel and aluminum cylinders are presented which show theoretical and experimental collapse pressures to agree within approximately 6 percent.

Using the theory developed in this report it is shown that a variation in stiffener size can change the buckling pressures. Test data from high-strength steel and aluminum cylinders are presented which show theoretical and experimental collapse pressures to agree within approximately 6 percent.

Using the theory developed in this report it is shown that a variation in stiffener size can change the buckling pressures. Test data from high-strength steel and aluminum cylinders are presented which show theoretical and experimental collapse pressures to agree within approximately 6 percent.

Using the theory developed in this report it is shown that a variation in stiffener size can change the buckling pressures. Test data from high-strength steel and aluminum cylinders are presented which show theoretical and experimental collapse pressures to agree within approximately 6 percent.

David Taylor Model Basin. Report 1600.
INVESTIGATION ON THE INFLUENCE OF STIFFENER SIZE ON THE BUCKLING PRESSURES OF CIRCULAR CYLINDRICAL SHELLS UNDER HYDROSTATIC PRESSURE, by James A. Nott. Dec 1961. ii, 63p. illus., graphs, tables, refs. UNCLASSIFIED

A theoretical derivation is given for elastic and plastic buckling of stiffened circular cylindrical shells under external hydrostatic pressure. The theory accounts for variable shell stresses, as influenced by the circular stiffeners, and critical buckling pressures are obtained for simple support conditions at the shell-frame junctures. Methods are given for the determination of collapse pressures for both elastic and plastic asymmetric buckling by iteration and numerical minimization. The theory is applicable to shells made either of strain-hardening or elastic-perfectly plastic materials.

1. Cylindrical shells (Stiffened)--Pressure--Measurement
2. Cylindrical shells (Stiffened)--Buckling--Measurement
3. Cylindrical shells (Stiffened)--Elasticity--Model tests
4. Cylindrical shells (Stiffened)--Failure

I. Nott, James A.
II. S-F013 03 02

David Taylor Model Basin. Report 1600.
INVESTIGATION ON THE INFLUENCE OF STIFFENER SIZE ON THE BUCKLING PRESSURES OF CIRCULAR CYLINDRICAL SHELLS UNDER HYDROSTATIC PRESSURE, by James A. Nott. Dec 1961. ii, 63p. illus., graphs, tables, refs. UNCLASSIFIED

A theoretical derivation is given for elastic and plastic buckling of stiffened circular cylindrical shells under external hydrostatic pressure. The theory accounts for variable shell stresses, as influenced by the circular stiffeners, and critical buckling pressures are obtained for simple support conditions at the shell-frame junctures. Methods are given for the determination of collapse pressures for both elastic and plastic asymmetric buckling by iteration and numerical minimization. The theory is applicable to shells made either of strain-hardening or elastic-perfectly plastic materials.

1. Cylindrical shells (Stiffened)--Pressure--Measurement
2. Cylindrical shells (Stiffened)--Buckling--Measurement
3. Cylindrical shells (Stiffened)--Elasticity--Model tests
4. Cylindrical shells (Stiffened)--Failure

I. Nott, James A.
II. S-F013 03 02

David Taylor Model Basin. Report 1600.
INVESTIGATION ON THE INFLUENCE OF STIFFENER SIZE ON THE BUCKLING PRESSURES OF CIRCULAR CYLINDRICAL SHELLS UNDER HYDROSTATIC PRESSURE, by James A. Nott. Dec 1961. ii, 63p. illus., graphs, tables, refs. UNCLASSIFIED

A theoretical derivation is given for elastic and plastic buckling of stiffened circular cylindrical shells under external hydrostatic pressure. The theory accounts for variable shell stresses, as influenced by the circular stiffeners, and critical buckling pressures are obtained for simple support conditions at the shell-frame junctures. Methods are given for the determination of collapse pressures for both elastic and plastic asymmetric buckling by iteration and numerical minimization. The theory is applicable to shells made either of strain-hardening or elastic-perfectly plastic materials.

1. Cylindrical shells (Stiffened)--Pressure--Measurement
2. Cylindrical shells (Stiffened)--Buckling--Measurement
3. Cylindrical shells (Stiffened)--Elasticity--Model tests
4. Cylindrical shells (Stiffened)--Failure

I. Nott, James A.
II. S-F013 03 02

David Taylor Model Basin. Report 1600.
INVESTIGATION ON THE INFLUENCE OF STIFFENER SIZE ON THE BUCKLING PRESSURES OF CIRCULAR CYLINDRICAL SHELLS UNDER HYDROSTATIC PRESSURE, by James A. Nott. Dec 1961. ii, 63p. illus., graphs, tables, refs. UNCLASSIFIED

A theoretical derivation is given for elastic and plastic buckling of stiffened circular cylindrical shells under external hydrostatic pressure. The theory accounts for variable shell stresses, as influenced by the circular stiffeners, and critical buckling pressures are obtained for simple support conditions at the shell-frame junctures. Methods are given for the determination of collapse pressures for both elastic and plastic asymmetric buckling by iteration and numerical minimization. The theory is applicable to shells made either of strain-hardening or elastic-perfectly plastic materials.

1. Cylindrical shells (Stiffened)--Pressure--Measurement
2. Cylindrical shells (Stiffened)--Buckling--Measurement
3. Cylindrical shells (Stiffened)--Elasticity--Model tests
4. Cylindrical shells (Stiffened)--Failure

I. Nott, James A.
II. S-F013 03 02

Using the theory developed in this report it is shown that a variation in stiffener size can change the buckling pressures. Test data from high-strength steel and aluminum cylinders are presented which show theoretical and experimental collapse pressures to agree within approximately 6 percent.

Using the theory developed in this report it is shown that a variation in stiffener size can change the buckling pressures. Test data from high-strength steel and aluminum cylinders are presented which show theoretical and experimental collapse pressures to agree within approximately 6 percent.

Using the theory developed in this report it is shown that a variation in stiffener size can change the buckling pressures. Test data from high-strength steel and aluminum cylinders are presented which show theoretical and experimental collapse pressures to agree within approximately 6 percent.

Using the theory developed in this report it is shown that a variation in stiffener size can change the buckling pressures. Test data from high-strength steel and aluminum cylinders are presented which show theoretical and experimental collapse pressures to agree within approximately 6 percent.

UNCLASSIFIED